https://doi.org/10.5194/egusphere-2024-3612
Preprint. Discussion started: 26 November 2024

Temperature variability in southern Europe over the past 16,500 years constrained by speleothem fluid inclusion water isotopes

Juan Luis Bernal-Wormull[1], Ana Moreno[1], Yuri Dublyansky[2], Christoph Spötl[2], Reyes Giménez[1], Carlos Pérez-Mejías[3], Miguel Bartolomé[4,5,6], Martin Arriolabengoa[7], Eneko Iriarte[8], Isabel Cacho[9], Richard Lawrence Edwards[10], and Hai Cheng[3,11,12]

[1] Department of Geoenvironmental Processes and Global Change, Pyrenean Institute of Ecology (IPE-CSIC), Avda. Montañana 1005, 50059 Zaragoza, Spain. jbernawo7@gmail.com; amoreno@ipe.csic.es; reiesgimenez@gmail.com

[2]Institute of Geology, University of Innsbruck, 6020 Innsbruck, Austria. yuri.dublyansky@uibk.ac.at; christoph.spoetl@uibk.ac.at

[3] Institute of Global Environmental Change, Xi'an Jiaotong University, Xi'an, 710049, China. perezmegias@xjtu.edu.cn; cheng021@xjtu.edu.cn

[4] Departamento de Geología, Museo Nacional de Ciencias Naturales (CSIC), C. de José Gutiérrez Abascal, 2, 28006 Madrid, Spain. mbartucar@gmail.com

[5] Swiss Institute for Speleology and Karst Studies (SISKA), Rue de la Serre 68, 2300 La Chaux-de-Fonds, Switzerland.

[6] Department of Earth Sciences, Geological Institute, NO G59, Sonneggstrasse 5, ETH, 8092 Zurich, Switzerland.

[7] Department of Geology, University of the Basque Country, Leioa, Spain. martin.arriolabengoa@ehu.eus

[8] Laboratory of Human Evolution-IsoTOPIK Stable Isotope Laboratory, Department of History, Geography & Communication, Edificio de I+D+i, Universidad de Burgos, Pl. Misael Bañuelos s/n, 09001, Burgos, Spain. eiriarte@ubu.es

[9] GRC Geociències Marines, Universitat de Barcelona, 28080 Barcelona, Spain. icacho@ub.edu

[10] Department of Earth and Environmental Sciences, University of Minnesota, Minneapolis, MN 55455, USA. edwar001@umn.edu

[11] State Key Laboratory of Loess and Quaternary Geology, Institute of Earth Environment, Chinese Academy of Sciences, Xi'an, 710061, China.

[12] Key Laboratory of Karst Dynamics, MLR, Institute of Karst Geology, CAGS, Guilin, 541004, China.

Correspondence: Ana Moreno (*amoreno@ipe.csic.es*)

https://doi.org/10.5194/egusphere-2024-3612
Preprint. Discussion started: 26 November 2024

ABSTRACT

In the Northern Hemisphere, the last 16.5 kyr were characterized by abrupt temperature transitions during stadials, interstadials, and the onset of the Holocene. These changes are closely linked to large-scale variations in the extent of continental ice-sheets, greenhouse gas concentrations, and ocean circulation. The regional impact of these rapid climate changes on Southwestern European environments is recorded by various temperature proxies, such as pollen and chironomids preserved in lake sediments. Speleothems and their fluid inclusions serve as valuable proxies, offering high-resolution chronologies and quantitative records of past temperature changes. These non-biogenic quantitative temperature records are essential to assess whether climate models can accurately simulate regionally divergent climatic trends and for understanding global and regional climate mechanisms in the past. Here, we present a record from five speleothems from two caves on the northeastern Iberian Peninsula (Ostolo and Medukilo caves). Using hydrogen isotopic composition of fluid inclusions, we developed a δ^2H/T transfer function in order to reconstruct regional temperatures over the past 16.5 kyr (Ostolo-Mendukilo Fluid Inclusion Temperature record [OM-FIT]). Our findings reveal an increase of 6.0 ± 1.9 ºC at the onset of Greenland Interstadial 1, relative to the cold conditions of the preceding Greenland Stadial 2.1a. Also, the OM-FIT record shows a temperature decline of approximately 5.3 ± 1.9 ºC during the early phase of Greenland Stadial 1. The end of this cold phase and the onset of the Holocene are marked by a rapid warming of about 3-4 °C and reaching a maximum at 11.66 ± 0.03 kyr BP. The OM-FIT record also exhibits abrupt events during the last deglaciation and the Holocene, which are also reflected in the δ^{18}O values of the calcite, including Heinrich Event 1, Greenland Interstadial 1d, and the 8.2 kyr event.

1. INTRODUCTION

The last deglaciation in the Northern Hemisphere (ca. 16.5 - 11.7 thousand years [kyr] BP - before present; present = 1950) was punctuated by a series of abrupt climatic changes driven by variations in the extent of large continental ice sheets, greenhouse gas concentrations, and deep-water ocean circulation (Clark et al., 2012). The Holocene was also characterized by variability in terms of temperature, precipitation seasonality, and glacier extent (Wanner et al., 2008, 2011), albeit at much smaller amplitudes compared to the Late Pleistocene. Reconstructing such paleoclimate changes quantitatively poses

https://doi.org/10.5194/egusphere-2024-3612
Preprint. Discussion started: 26 November 2024

significant challenges due to the scarcity of quantitative techniques and the fact that proxy signals in archives may be influenced by more than one meteorological variable (e.g., temperature and precipitation), which complicates our understanding of past temperature variations (Heiri et al., 2014a; Moreno et al., 2014). These limitations greatly hinder the assessment of whether reconstructed paleotemperatures in different regions are reflecting climate variations or different methodologies. Therefore, it is crucial to obtain proxy data that accurately reflect quantitative changes in paleotemperature, independent of past changes in rainfall or humidity. Quantitative temperature reconstructions are needed to assess the ability of climate simulation models to predict regionally divergent trends in climate change and to better understand the mechanisms of global and regional climate variability (e.g., Affolter et al., 2019).

The last deglaciation in the Northern Hemisphere involved major climatic shifts associated with Greenland Stadials (GS-2.1a and GS-1) and Interstadials (GI-1 and the onset of the Holocene). The impact of these rapid climate changes on Southwestern European environments is recorded by temperature proxies, e.g., pollen, speleothems, planktonic foraminifera, and chironomids (Millet et al., 2012; Heiri et al., 2014b; González-Sampériz et al., 2017; Tarrats et al., 2018; Català et al., 2019; Cheng et al., 2020). However, the available temperature reconstructions exhibit large regional climate differences across Europe (Renssen and Isarin, 2001; Heiri et al., 2014b; Affolter et al., 2019). For example, the chironomid study by Heiri et al. (2014b) revealed that temperature variations during the last deglaciation were more pronounced in Western Europe than in Southwestern, Central, and Southeastern Europe. Similar regional disparities are observed during the Holocene, where the long-term evolution of global and hemispheric temperature variations remains a subject of debate, with climate models and proxy records showing differing trends (Marcott et al., 2013; Shakun, 2018; Affolter et al., 2019). Given these uncertainties, quantitative studies using inorganic archives, such as fluid inclusions (FI) in speleothems (Dublyansky and Spötl, 2009; Demény et al., 2016, 2021) are gaining increasing relevance (Affolter et al., 2019; Wilcox et al., 2020; Honiat et al., 2023) as a complement to existing studies largely based on biological archives. The strengths of this method are: (a) the accurate and precise chronology provided by speleothems, (b) the well-established link between cave interior temperature and mean outside air temperature, and (c) the relationship between temperature and water isotopes, which is controlled by physical rather than biological processes. FI water isotopes can be measured using different analytical techniques (Vonhof et al., 2006; Dublyansky and Spötl, 2009; Arienzo et al., 2013; Affolter et al., 2014) and FI-based paleotemperature reconstruction methods (Demény et al., 2016, 2021; Uemura et al., 2020). One such approach is based on the δ^2H_{FI} composition and uses the δ^2H_{FI}-temperature relationship determined for a given study area (Affolter et al., 2019). The principal advantage of this method lies in its reliance on a relatively simple and robust analytical method. The δ^2H_{FI}-temperature relationship is established using monitoring data, and the approach is most effective in settings where δ^2H variability in rainfall is driven by surface temperature (Demény et al., 2021). For the FI water isotope thermometry method to yield reliable results, four aspects must be considered: (i) FIs must be of primary origin, well-sealed, and sufficiently abundant; (ii) the choice of the transfer function converting the hydrogen and/or oxygen isotope signal (δ^2H_{FI}, $\delta^{18}O_{FI}$) into temperature may bias temperature estimates; (iii) the relationship between δ^2H_{FI} and $\delta^{18}O_{FI}$ may have changed over time; and (iv) the FI water isotope method assumes that speleothem calcite was deposited under isotopic equilibrium conditions.

Here, we assess the air temperature evolution in the northern Iberian Peninsula over the last 16.5 kyr using quantitative FI-based data from five well-dated stalagmites that overlap during the last deglaciation and Holocene, showing very similar stable isotope trends. This record (dubbed OM-FIT) in conjunction with other regional terrestrial proxy records allows to better disentangle the effects of temperature and humidity reported by previous studies using calcite stable isotope data from caves in southwestern Europe (Bernal-Wormull et al., 2021, 2023). The paleotemperature data obtained from FIs in speleothems represent the first quantitative air temperature reconstruction for northeastern Iberia during the last deglaciation and provide a basis for future studies aiming to enhance our quantitative understanding of rapid regional climate changes.

2. STUDY SITES

2.1. Ostolo and Mendukilo caves

Ostolo (43°11'16"N, 1°43'56"W, 248 m a.s.l.) and Mendukilo (42º58'25"N, 1º53'45"W, 750 m a.s.l.) caves are located in northern Iberia (Fig. 1). Although only about 28 km apart, they exhibit different geological, geomorphological, and climatic settings. Ostolo cave is located in the Bidasoa river valley, formed within the Carboniferous limestones of the Cinco Villas Massif (Basque Mountains, Western Pyrenees). Mendukilo cave, on the other hand, is developed in Lower Cretaceous limestones (Urgonian, Albian-Aptian) along the eastern boundary of the Basque-Cantabrian basin. For additional details on the caves and the locations of the sampled stalagmites, see Bernal-Wormull et al. (2021, 2023).

The climate in the study region is dominated by the Atlantic Ocean, characterized by temperate summers, evenly distributed rainfall throughout the year, and no distinct dry season (Cfb of the Köpper-Geiger climate classification). Mediterranean fronts may also be secondarily responsible for rainfall. Mean annual air temperature (MAAT) and mean annual precipitation are higher in the Ostolo cave area (13.5 ± 0.8 °C; >2000 mm/year) compared to Mendukilo (12.2 ± 0.4 °C; ~1365 mm/year). This temperature difference is even more pronounced inside the caves: the average annual cave air temperature in Ostolo is 13 ºC, while in Mendukilo, it is 8.8 ºC. The lower temperature inside Mendukilo is due to its more closed and hence less ventilated nature compared to Ostolo, which also contains a cave stream that helps stabilize its internal temperature (Bernal-Wormull et al., 2021). In contrast, the "cold-trap" behavior of Mendukilo is consistent with its more complex geometry, resulting in an anomalously low temperature (Bernal-Wormull et al., 2023). The vegetation around both caves is dominated by oak (*Quercus robur* and *Quercus pyrenaica*), alder (*Alnus glutinosa*), beeche (*Fagus sylvatica*), as well as Atlantic-type polycultures, ferns, and heathers.

2.2. Isotopic composition of drip waters in Ostolo and Mendukilo

Quantitative reconstruction of past climate variability from speleothem isotope records relies on understanding the modern vadose karst flow regime (Lachniet, 2009). For Mendukilo, the $\delta^{18}O$ and $\delta^{2}H$ values of drip waters feeding the stalagmites studied here remain relatively constant, with mean values of −7.7 ± 0.4‰ and −45.3 ± 2.9‰ Vienna Standard Mean Ocean Water (VSMOW), respectively (1σ uncertainty), and lack of a seasonal pattern (Bernal-Wormull et al., 2023). The monitoring period in Mendukilo cave lasted nearly three years, with measurements taken every 2-3 months (2018-2021). In Ostolo, the $\delta^{18}O$ and $\delta^{2}H$ values of drip water are also similarly stable, with mean values of −6.3 ± 0.2‰ and −37.8 ± 1.6‰ VSMOW, respectively, with carbonate precipitation throughout the year in only one gallery of the cave (Bernal-Wormull et al., 2021). The monitoring interval in Ostolo was 3-4 months over one year (2019-2020).

2.3. Isotopic composition of rainfall

The rainfall stable isotopic composition near the study sites was analyzed by Giménez et al. (2021) on an event basis above "Las Güixas" cave (Villanúa village), approximately 100 km east of the Ostolo and Mendukilo caves. This show cave, located in the Central South Pyrenees (Fig. 1), experiences a transitional Mediterranean-Oceanic climate (Cfb of the Köpper-Geiger climate classification) with a MAAT of 11 ºC and around 1100 mm of annual precipitation. During the winter the westerly winds and Atlantic fronts are responsible for most rainfall, while rest of the year is mixed between Mediterranean and Atlantic fronts (Giménez et al., 2021), similar to the conditions in the area of Ostolo and Mendukilo caves. Two years of stable isotope data in precipitation and air temperature on an event scale are available from this station (2017-2019, Giménez et al., 2021). The weighted mean values of $\delta^{18}O$ and $\delta^{2}H$ are −7.8 ± 4.3‰ and −54.5 ± 32.9‰, respectively, with seasonal variations reaching total amplitudes of 23 and 174‰, respectively (Giménez et al., 2021). The Local Meteoric Water Line (LMWL) is defined as $\delta^{2}H = 7.56 \cdot \delta^{18}O + 4.33$ (n = 210; $R^2 = 0.97$). The slope of the LMWL is close to that of the Global Meteoric Water Line (GMWL; Rozanski et al., 1993) and aligns well with the water line defined by the drip waters of Mendukilo and Ostolo caves (Fig. 2A). In general, the isotopic composition of rainfall correlates with air temperature for the 2-year period (n =210; $R^2 = 0.44$, Fig. 2B), and show moderate correlation with relative humidity and a weaker correlation with rainfall amount at event scale when performing a Spearman's correlation (r_s; n = 180; between rainfall amount and $\delta^{18}O$ [$\delta^{2}H$]: $r_s = -0.27$ [−0.25]; between temperature and $\delta^{18}O$ [$\delta^{2}H$]: $r_s = 0.70$ [0.69]; between relative humidity at the rainfall site and $\delta^{18}O$ [$\delta^{2}H$]: $r_s = -0.46$ [−0.41]) (Giménez et al., 2021).

3. METHODS

3.1 Sampling and petrography

Stalagmites OST1, OST2 and OST3 were retrieved from a gallery in Ostolo cave, where active speleothem deposition was not observed. Stalagmites MEN-2 and MEN-5 were retrieved from a gallery in Mendukilo cave, where active calcite precipitation was only observed at the original dripping point of MEN-5. See Bernal-Wormull et al. (2021, 2023) for more details on these caves. All stalagmites were cut longitudinally and the central slab was polished. Small blocks were cut along the growth axis for the preparation of doubly-polished thin sections (about 200 μm). FIs were studied in these thin sections using a Nikon Eclipse transmitted-light microscope.

3.2. FI stable isotopic composition

A total of 344 carbonate subsamples (including duplicates) were crushed and analyzed for δ^2H_{FI} (287 subsamples of Mendukilo stalagmites and 69 of Ostolo samples). Between 0.3 and 2.5 g of calcite were used to ensure a sufficiently high water yield (0.1-1 μL). Stable isotope measurements were performed using a Delta V Advantage isotope ratio mass spectrometer, following the methodology described by Dublyansky and Spötl, (2009). δ^2H_{FI} values are reported in per mil relative to VSMOW. The average long-term precision of replicate measurements of an in-house calcite standard is ±2.7 ‰ for δ^2H_{FI} for water amounts between 0.1 and 1 μL.

δ^2H_{FI} is regarded as a more robust proxy of paleotemperature than $\delta^{18}O_{FI}$, as it is less influenced by non-climatic parameters, with no other sources of hydrogen affecting the water trapped in the calcite (Demény et al., 2016, 2021; Affolter et al., 2019). In addition, $\delta^{18}O_{FI}$ values obtained with the Innsbruck FI setup can be inaccurate for samples of low water content (<0.1 μL; Dublyansky and Spötl, 2009). Therefore, we only used δ^2H_{FI} values in this study.

4. RESULTS

4.1. Petrography

The Ostolo and Mendukilo stalagmites consist of coarse crystalline calcite and are macroscopically homogenous without any sign of recrystallization. The MEN-2 and MEN-5 stalagmites exhibit a columnar fabric, lack growth hiatuses, and do not show macroscopically visible laminae (Bernal-Wormull et al., 2023). In contrast, the Ostolo stalagmites shows a more porous columnar microcrystalline fabric that transitions into an elongated-columnar type (Bernal-Wormull et al., 2021). Two hiatuses are present in OST3, marked by organic inclusions and micrite layers.

Primary FIs were observed in all stalagmites samples (Fig. 3). The Mendukilo samples contain considerably more FIs compared to those from Ostolo, mainly concentrated along growth layers (Fig. 3A). In the Mendukilo stalagmites, primary inter-

https://doi.org/10.5194/egusphere-2024-3612
Preprint. Discussion started: 26 November 2024

crystalline (10-30 μm; Fig. 3B) and intra-crystalline (10 to >100 μm; Fig. 3C) FIs are discernible. These intra-crystalline primary FIs are elongated and rounded or pyriform in shape (rounded at the base with a spike extending in the speleothem growth direction; Fig. 3C; Lopez-Elorza et al., 2021). In Ostolo, FIs are less prominent and are mostly intra-crystalline, located along or around white porous laminae and within the more elongated columnar or microcrystalline fabrics (Fig. 3D, E). The intra-crystalline FIs in Ostolo samples are, on average, smaller than those in the Mendukilo stalagmites (10-40 μm) and predominantly exhibit pyriform or rounded shapes (Fig. 3F). Petrographic observations confirm that the FIs in these samples are primary, well preserved, and suitable for their stable isotopic analysis.

4.2. Last deglaciation and Holocene $\delta^{18}O$ speleothem record

The chronology of the Ostolo stalagmites spans the last deglaciation between 16.5 and 11.7 kyr BP with high precision due to their very high ^{238}U concentrations (10-80 ppm). The carbonate $\delta^{18}O$ ($\delta^{18}O_c$) profiles show consistency among the three stalagmites (Fig. 4). OST1 and OST2 have more negative values (−5 to −8.9‰) during GS-1 and GS-2.1a, and less negative values (up to −3.4‰) during GI-1 and the onset of the Holocene. OST3 did not grow during the intervals characterized by the most negative $\delta^{18}O_c$ values recorded by the other two stalagmites (Fig. 4). On the other hand, the MEN stalagmites, despite having lower ^{238}U concentrations (100-350 ppb), also have lower detrital ^{232}Th contents, enabling robust age models for both stalagmites. These models cover various intervals of the Holocene and GS-1 with good overlap (Fig. 4), specifically: (i) MEN-2 grew between 12.8 and 6.3 kyr BP, with $\delta^{18}O$ values that remain stable during GS-1, followed by an abrupt increase, reaching the highest values of the entire record at the GS-1/Holocene transition (from −5.2‰ in GS-1 to −4.3‰ at 11.6 kyr BP). (ii) MEN-5 spans the last 8.8 kyr and presents prominent negative values during certain short events (e.g., 8.2 kyr BP with a value of −6.3‰, replicated by MEN-2), which are synchronous, within age uncertainties, with abrupt changes in the isotopic composition of North Atlantic surface waters (Kleiven et al., 2008; Carlson et al., 2008). More details on the chronology and isotopic data of these speleothems are provided by Bernal-Wormull et al. (2021, 2023).

4.3. FI isotopes

OST samples are characterized by variable water content, with replicates yielding a mean standard deviation of ±2.7‰ for δ^2H. We assigned this value to individual measurements as an overall uncertainty estimate. Not all OST samples could be duplicated due to sometimes low water amounts and petrographically complex FI assembles in some samples (Fig. 3D, E), which restricted subsampling of some individual growth layers. All MEN measurements were duplicated, triplicated, or even quadruplicated. The δ^2H values of sub-samples of MEN-2 and MEN-5 (ranging between −34 and −61‰) with water contents of 0.1 to 1 µL replicated within 2.7‰.

δ^2H_{FI} values for the Holocene and GI-1 are comparable to cave drip waters at Mendukilo and Ostolo caves (Fig. 4). In contrast, values are more negative during GS-1 and GS-2.1a (Fig. 4). GS-2.1a is represented by 8 OST subsamples with a mean δ^2H_{FI} value of −58‰. One of these values, dated to 15.80 ± 0.05 kyr BP, is even more depleted (−66.8 ± 2.4‰). Values become less negative rapidly at 14.57 ± 0.05 kyr BP (Fig. 4; mean during GI-1: −40‰). This trend is interrupted in the three OST stalagmites at 14.13 ± 0.09 kyr BP, leading to more negative values (between −40 and −56‰). During GS-1, the δ^2H_{FI} values decrease again (Fig. 4), averaging −51‰ before showing a rapid increase at the onset of the Holocene (−36‰). The MEN-2 record also shows a mean of −51‰ during GS-1, though the transition to the Holocene is more gradual. Between 8.7 and 6.3 kyr BP, MEN-2 and MEN-5 δ^2H_{FI} values show excellent correlation (Fig. 4). There is no significant variation between the Greenlandian (−44‰), Northgrippian (−43‰), and Meghalayan (−42‰). Despite these relatively stable δ^2H_{FI} values throughout the Holocene substages, a short negative shift is identified at 8.29 ± 0.07 (−54.9 ± 6.5‰) kyr BP.

5. DISCUSSION

5.1. Interpretation of the δ^{18}O signal

Variations in stalagmite $\delta^{18}O_c$ records may reflect changes in the δ^{18}O of surface ocean waters from the moisture source area as well as changes in atmospheric processes which control the fractionation of oxygen isotopes in route to the site where rainfall occurs (McDermott, 2004; Lachniet, 2009). In the Ostolo stalagmites, the $\delta^{18}O_c$ signal is coherent with air temperature changes throughout the deglaciation period (Bernal-Wormull et al., 2021). The overall $\delta^{18}O_c$ pattern observed in these stalagmites is similar to that of speleothems from the Pyrenees (Bartolomé et al., 2015; Cheng et al., 2020) and the Alps (Luetscher et al., 2015; Li et al., 2020), which also predominantly receive Atlantic-derived moisture and where $\delta^{18}O_c$ primarily reflects atmospheric temperature. Superimposed on the temperature effect are changes in the isotopic composition of seawater, which may account for the negative excursion in the Ostolo $\delta^{18}O_c$ record during Heinrich event 1 (HE1) at 16.2–16.0 kyr BP, with values reaching as low as −8.9‰ (Bernal-Wormull et al., 2021; Fig. 4).

Conversely, the MEN $\delta^{18}O_c$ record captures a temperature signal that is obscured by the influence of rainfall amount, since temperature and humidity changes may have competing effects on the $\delta^{18}O_c$ signal (Bernal-Wormull et al., 2023). Additionally, during the earlier part of the record (13-8 kyr BP), changes in the oceanic isotopic composition associated with meltwater input (Skinner and Shackleton, 2006; Eynaud et al., 2012) that further affect the signal. A prominent feature of the MEN-2 and MEN-5 $\delta^{18}O_c$ records is a −0.7‰ anomaly (relative to the Holocene mean of −5.4‰) observed at 8.11 and 7.00 kyr BP (Fig. 4). These two events of anomalously low $\delta^{18}O_c$ values likely reflect rapid, short-lived decreases in temperature and in the $\delta^{18}O$ of the surface ocean water, rather than increased rainfall, as proposed in previous studies (e.g., LeGrande and Schmidt, 2008; Domínguez-Villar et al., 2009; Matero et al., 2017; García-Escárzaga et al., 2022).

5.2. Isotope-temperature conversion

The composite paleotemperature records of the Ostolo and Mendukilo speleothems are based on 356 FI samples (and replicates), applying a regional water isotope-temperature relationship derived from monitoring data (isotopic data of drip water and outside temperature) of both caves (Bernal-Wormull et al., 2021, 2023) and the relationship between rainfall δ^2H (δ^2H_r) and modern air temperature. The latter provides a relationship between air temperature and the stable isotopic composition of rain ($\delta^{18}O_r$ and δ^2H_r) observed from July 2017 to June 2019 (n = 210). The observed correlation between $\delta^{18}O$ and air temperature is verified at biannual scale, with significant correlation between MAAT and the weighted average $\delta^{18}O_r$, based on a multiple regression model using a univariate Spearman's correlation between $\delta^{18}O_r$ and air temperature at the time of precipitation (same data series), that also accounts for rainfall amount and relative humidity ($r_s = 0.7$; $p << 0.01$, Giménez et al., 2021).

https://doi.org/10.5194/egusphere-2024-3612
Preprint. Discussion started: 26 November 2024

$\delta^{18}O$ and δ^2H values of seawater vary on glacial-interglacial timescales due to the ice-volume effect: When surface waters evaporates from the ocean, lighter stable isotopes are preferentially removed into the vapor phase, leading to increased $\delta^{18}O$ and δ^2H values in the ocean water as more fresh water is stored as ice on continents (Lachniet, 2009). δ^2H_{FI} values were corrected for the ice-volume effect during the deglaciation period covered by the MEN and OST speleothems. This correction used a gradient derived for $\delta^{18}O$ (Bintanja et al., 2005) converted to δ^2H using a factor of eight. Paleotemperatures were then estimated using a linear δ^2H/T transfer function anchored to the MAAT at both cave sites and the isotopic composition of drip water (δ^2H_d; Ostolo δ^2H_d = −37.8‰; Mendukilo δ^2H_d = −45.3‰), with corrections for the elevation of the Villanúa monitoring station (950 m a.s.l.). The modern δ^2H values were adjusted for the elevation difference between the rainfall sampling station and the studied caves, assuming a lapse rate of 0.2‰ per 100 m for $\delta^{18}O$, i.e., 1.6‰ per 100 m for δ^2H_p (Poage, 2001). The uncertainties associated with δ^2H_{FI}, δ^2H_d, δ^2H/T, and MAAT, as well as the slope of the LMWL, were propagated through the calculation steps. Due to a lack of constraints on past seasonal changes in precipitation and effective infiltration, we assume constant annual infiltration over time.

5.3. OM-FIT: paleothermometric record derived from FI stable isotope data

Our δ^2H_{FI} values provides a robust record, because: (i) part of the record is well replicated by samples from two caves from different climatic settings (e.g., during the Younger Dryas [YD]), (ii) stalagmites from the same cave are replicated (within their respective uncertainties), and (iii) a large proportion of the samples have multiple replications. We investigated the temperature dependence of the hydrogen (and oxygen) isotope composition of precipitation water in the study region, examining the modern-day δ^2H/T and $\delta^{18}O/T$ gradients. This relationship, which may change over time, was examined by Rozanski et al. (1992) for Central Europe and applied by Affolter et al. (2019) to a 14 kyr record from Milandre cave (Switzerland). It was similarly applied to Last Interglacial records from Alpine caves (Wilcox et al., 2020; Honiat et al., 2023). The relationship between mean annual $\delta^{18}O_r$ and MAAT ($\delta^{18}O/T$) is 0.55 ± 0.03‰ °C^{-1} for the "Las Güixas" tourist cave in Villanúa, which is consistent with the average European $\delta^{18}O/T$ gradient of 0.59 ± 0.08‰ °C^{-1} (Rozanski et al., 1992). The OST and MEN FI isotope data overlap chronologically for the YD, allowing for their combination into a

https://doi.org/10.5194/egusphere-2024-3612
Preprint. Discussion started: 26 November 2024

single temperature transfer function (OM-FIT) covering the last 16.7 kyr BP (Fig. 5). The OM-FIT is calculated using the corrected δ^2H_{FI} values, δ^2H_d, MAAT (T_{modern}), and the modern-day δ^2H/T gradient derived from the LMWL of rainfall isotopes:

$$T_{OM-FIT} = T_{modern} - \frac{\delta^2H_d - \delta^2H_{FI\,(corrected)}}{\delta^2H/T_{gradient}} \quad (1)$$

As explained above in chapter 5.2, the $\delta^{18}O$ values were further adjusted using the equilibrium fractionation factor of eight to elaborate the temperature reconstruction exclusively with δ^2H data. The temperature reconstruction with Equation (1) is based on the mean relationship of 4.4‰/°C (for δ^2H). The final calculated uncertainty in the paleotemperature ranges from 1.8 to 3.0 ºC.

5.4. Temperature regime of Northern Spain based on OM-FIT

5.4.1. Last deglaciation

The Ostolo cave $\delta^{18}O_c$ and δ^2H_{FI} records (Fig. 4) and the OM-FIT (Fig. 5) show clear evidence of rapid temperature changes during GS-2.1a, GI-1, GS-1, and the onset of the Holocene. The timing and amplitude of these changes are in well agreement with other European oxygen isotope records from lake sediments (Von Grafenstein et al., 1999; Van Raden et al., 2013) and speleothems (Luetscher et al., 2015; Affolter et al., 2019; Cheng et al., 2020; Li et al., 2020). The strong similarity between these records and NGRIP $\delta^{18}O$ (Rasmussen et al., 2014) and temperature reconstructions (Kindler et al., 2014) (Fig. 6) supports the idea of a common North Atlantic climate forcing during the last deglaciation on millennial to centennial timescales.

The OM-FIT record suggests that regional MAAT during GS-2.1a was slightly lower than during GS-1, characterized by a negative excursion at 15.8 ± 0.1 kyr BP and a temperature decrease of approximately 2.0 °C relative to the GS-2.1a average (Fig. 5). This OM-FIT anomaly corresponds with the final phase of HE1, related to massive iceberg discharges from the Laurentide ice sheet, which collapsed around 16.2 ± 0.3 kyr BP (Landais et al., 2018). Regionally, a significant glacier advance occurred at that time in the Pyrenees and other Iberian mountains (García-Ruiz et al., 2023), and speleothems from Meravelles cave (NE Iberia) record a notable $\delta^{18}O_c$ anomaly between 16.2 and 15.9 kyr BP (Pérez-Mejías et al., 2021). This anomaly appears to reflect changes in the isotopic composition of the moisture source, contributing to the negative excursion in the OST2 $\delta^{18}O_c$ record between 16.2 and 16.0 kyr BP (Bernal-Wormull et al., 2021; Fig. 5). This observation confirms that the OM-FIT record captured not only temperature history on millennial scales but also abrupt climate events on a centennial scale.

A rapid temperature increase of 6.0 ± 2.1 °C occurred at the onset of GI-1 (Fig. 5). This increase in the OM-FIT record coincides with an important glacier retreat in the Iberian mountains (García-Ruiz et al., 2023), an increase in chironomid-inferred July air temperatures (from ca. 11 °C to ca. 16 °C) from the west-central Pyrenees (Millet et al., 2012), and an increase in MAAT (from ca. 12.2 °C to ca. 18.6 °C) recorded by branched glycerol dialkyl glycerol tetraethers in the Padul palaeolake record (Sierra Nevada, southern Iberian Peninsula; Rodrigo-Gámiz et al., 2022). The onset of GI-1 in the OM-FIT was recorded by δ^2H_{FI} data from the OST1 and OST3 stalagmites. The amplitude of this abrupt warming is in agreement with other European temperature records, such as estimates based on $\delta^{18}O_c$ data from Alpine speleothems (Luetscher et al., 2015; Li et al., 2020). Von Grafenstein et al. (2013) used a combination of ostracod, mollusc, and charophyte data to estimate a rise of about 6 °C in MAAT for this transition at the Gerzensee lake site. The Ammersee record, using a coefficient derived from a study of northern Switzerland stalagmites (0.48‰/°C, Affolter et al., 2019), estimated a warming of about 5.5 °C (4.1–8.4 °C) (Li et al., 2020) for this transition.

During GI-1, the δ^2H_{FI} record is marked by higher δ^2H values and similar temperatures in the OM-FIT record compared to the onset of the Holocene (Fig. 5). As observed in the OST $\delta^{18}O_c$ record, δ^2H_{FI} values follow a negative trend towards the end of GI-1. Within this interstadial, a significant inflection point occurs with a negative anomaly at 14.1 ± 0.1 kyr BP in the OM-FIT record. This suggests that the OM-FIT minimum during GI-1, also registered at 14.10 ± 0.03 kyr BP in the OST $\delta^{18}O_c$ record and equivalent to GI-1d in NGRIP (Rasmussen et al., 2014), involved the most pronounced cooling of GI-1 (between 3.0 and 3.7 ± 2.1 °C in the OM-FIT record), occurring just after the GI-1e warm phase (Fig. 5). This cooling event is contemporaneous with glacier expansions in the Pyrenees (García-Ruiz et al., 2023) and a centennial-scale cooling at Ech paleolake (Millet et al., 2012), Lake Estanya (Vegas-Vilarrúbia et al., 2013) and in the Portalet sedimentary sequence (González-Sampériz et al., 2006). Apparently, this relatively small decrease in temperature during GI-1d, as quantified by the OM-FIT record and chironomid-inferred July air temperatures (Millet et al., 2012) in this region, resulted in (i) an important vegetation response (González-Sampériz et al., 2017), characterized by a decrease in juniper and an expansion of steppe herbs during this cold and dry event, and (ii) carbonate and massive organic-rich silt deposition during warm and humid interstadials alternating with siliciclastics under cold and arid conditions (González-Sampériz et al., 2006).

Between 13.0 and 12.5 kyr B.P., the δ^2H_{FI} decrease (Fig. 4) records a cooling of 5.5 ± 2.1 ºC in the OM-FIT record (Fig. 5), marking the initial part of GS-1 (Rasmussen et al. 2014). Similar cooling magnitudes were reported for the central Pyrenees (Bartolomé et al., 2015). On the other hand, this change appears slightly larger compared to cooling registered by summer air temperature records of the GI-1/GS-1 transition, such as those from lake sediments in NW Iberia (2-3 ºC; Muñoz Sobrino et al., 2013) and the central Pyrenees (1.5-2 ºC; Millet et al., 2012). This important change in the OM-FIT record also agrees in magnitude with a rapid cooling recorded by (i) speleothems from the Alps (around 4–5 °C; Li et al., 2020) and the Jura Mountains (4.3 ± 0.8 °C; Affolter et al., 2019), and (ii) a drop in sea-surface temperatures of around 4 °C off the Iberian coast at 12.9 kyr BP (Rodrigues et al., 2010; Martrat et al., 2014).

The end of the GS-1 cold phase and the onset of the Holocene are marked by a rapid warming in the OM-FIT record of about ~4 °C (Fig. 5), peaking at 11.67 ± 0.02 kyr BP. The variability of MEN $\delta^{18}O_c$ data during the GI-1/GS-1 and GS-1/Holocene onset transitions is less pronounced compared to OST $\delta^{18}O_c$. This observation may be due to the proximity of Mendukilo cave to the Atlantic coast, with temperature and humidity changes having competing effects on $\delta^{18}O_c$, as already reported in other speleothem records from this region (e.g., Baldini et al., 2019). In contrast, the $\delta^{18}O_c$ of speleothems from Pyrenean caves is predominantly controlled by temperature (Bartolomé et al., 2015; Cheng et al., 2020; Bernal-Wormull et al., 2021), resulting in a more "smoothed" temperature signal compared to the OST $\delta^{18}O_c$ record during GS-1, a cold and dry period (Fletcher et al., 2010). Nevertheless, the MEN δ^2H_{FI} records captures important changes during the GI-1/GS-1 and GS-1/Holocene transitions and correlates quite well with the δ^2H_{FI} data from OST (Fig. 4).

5.4.2. Holocene

As mentioned above, the Holocene section of the OM-FIT record (Fig. 5) is based on δ^2H_{FI} values of the MEN stalagmites (Fig. 4). This record not only captures variability in

https://doi.org/10.5194/egusphere-2024-3612
Preprint. Discussion started: 26 November 2024

$\delta^{18}O_c$ composition influenced by temperature but also reflects past hydroclimatic conditions (Bernal-Wormull et al., 2023). This observation introduces a limitation in reconstructing periods of relatively stable temperature, such as the Holocene, which is represented by centennial-scale OM-FIT temperature variability that reaches up to 2 °C in certain intervals. However, these variations are close to the uncertainty range of the OM-FIT record (± 1.8 °C to ± 3.0 °C for the Holocene). Therefore, these reconstructed quantitative temperature data for the Holocene must be viewed with caution. On millennial scales, the OM-FIT record shows peak temperatures during the onset of the Holocene (until ~10 kyr BP), albeit with high variability. This early rapid warming is also recorded by the hydroclimate-sensitive isotopic signal of the SIR-1 stalagmite from NW Iberia (Rossi et al., 2018). This observation underscores the value of obtaining a temperature-sensitive record in regions where the isotopic signal of speleothems is also influenced by the amount effect, such as the MEN $\delta^{18}O_c$ record.

The OM-FIT record does not capture a clear cooling trend after the Holocene Thermal Maximum (HTM) compared to the $\delta^{18}O$ record from Greenland ice cores (Rasmussen et al., 2014) and the Milandre cave fluid inclusion temperature record (MC-FIT) record from central Europe (Affolter et al., 2019) (Fig. 6), instead suggesting stable temperatures. This Neoglacial cooling, widespread across the Northern Hemisphere, is well documented throughout Europe (e.g., Larocque-Tobler et al., 2010; Ilyashuk et al., 2011) and Iberia (Sancho et al., 2018; Leunda et al., 2019; Català et al., 2019; García-Ruiz et al., 2020). The absence of this cooling in the OM-FIT record is likely due to masking by large centennial variability and large temperature uncertainties. The temperature trends in MEN $\delta^{18}Oc$ and OM-FIT differ from those captured by chironomids in the central Pyrenees (Tarrats et al., 2018), which indicate a millennial-scale cooling during the middle Holocene compared to the HTM and the late Holocene (Fig. 6). This observation highlights the differences between temperature records derived from speleothems (OM-FIT, without seasonal bias) and chironomids (recording summer air temperature), as in the case for GS-1.

Despite the limited precision of OM-FIT, it can identify abrupt centennial events, some of which are also evident in the $\delta^{18}Oc$ values of MEN-2 and MEN-5 (Fig. 6). For example, one of the lowest OM-FIT temperatures (9.8 ºC) occurred at 11.50 ± 0.08 kyr BP (mean temperature at the onset of the Holocene, 12.3 ± 1.8 ºC), corresponding within age uncertainties to the Preboreal Oscillation (11.4 kyr) recorded in Greenland ice cores

(11.27 ± 0.03 kyr BP, based on the new ice core chronology - Seierstad et al., 2014) and by MC-FIT in Switzerland (11.37 ± 0.15 kyr BP - Affolter et al., 2019) (Fig. 6). Another example is the 9.2-kyr event, documented across the Northern Hemisphere (e.g., Masson-Delmotte et al., 2005; Genty et al., 2006; Rasmussen et al., 2007; Fleitmann et al., 2008) ans supported by terrestrial (Carrión, 2002; Vegas et al., 2010; Iriarte-Chiapusso, 2016; Mesa-Fernández et al., 2018; Baldini et al., 2019) and marine records from Spain (Nebout et al., 2009). This event is captured by a δ^2H_{FI} value of −51‰ in MEN-2 and an OM-FIT temperature of 10.4 ± 1.9 ºC at 9.29 ± 0.08 kyr BP (Fig. 6). However, it is absent from the $\delta^{18}O_c$ record of MEN-2, and previous research suggests that the climate in northern Spain was likely considerably warmer and wetter ~9 ka BP (Morellón et al., 2018; Tarrats et al., 2018; Baldini et al., 2019). This observation supports the assertion of Bernal-Wormull et al. (2023) that the less variable $\delta^{18}O_c$ signal in Mendukilo cave is influenced not only by short-lived decreases in $\delta^{18}O_{sw}$ but also by changes in humidity.

Catastrophic meltwater discharge during the '8.2 kyr event' from glacial lake Agassiz lowered the isotope composition of North Atlantic surface water by 0.4‰ (Kleiven et al., 2008; Carlson et al., 2008) and led to a wide-spread cooling across the circum-North Atlantic. The isotopic signal of this meltwater event was transported by the westerlies and left an imprint in the isotopic composition of precipitation in Iberia (LeGrande and Schmidt, 2008; Bernal-Wormull et al., 2023). The 8.2-kyr event overlapped a multi-centennial cool period from 8.29 to 8.10 ± 0.04 kyr BP recorded by MEN $\delta^{18}O_c$, characterized by an abrupt drop in temperature of about ~2.7 ºC between 8.31 ± 0.06 and 8.29 ± 0.07 kyr BP in the OM-FIT record (Fig. 6). This cooling within an interglacial coincided with significant vegetation changes in the Iberian Peninsula (Allen et al., 1996; Carrión and Van Geel, 1999; González-Sampériz et al., 2006). This could be important for assessing future climate conditions in this region if changes in large parts of the climate system (climate tipping elements; Armstrong McKay et al., 2022) intensify beyond a warming threshold.

The cooling amplitude during the 8.2 kyr event recorded by OM-FIT appears more pronounced than in other Northern Hemisphere temperature and precipitation records, with proxy evidence across Europe indicating a cooling by ~ 1-1.7 ºC during this event (Davis et al., 2003; Morrill et al., 2013; Baldini et al., 2019). Other terrestrial records in southwestern Europe offer important insights into the paleoenvironment during this event (e.g., Fletcher et al., 2013; González-Sampériz et al., 2017; Morellón et al., 2018;

Zielhofer et al., 2019). Some records often present conflicting insights on humidity conditions due to the exposure of this study region to both Mediterranean and North Atlantic air masses (Moreno et al., 2017, 2021). However, most of these terrestrial records capture broader climate shifts, often lacking the resolution to fully constrain the regional response to the 8.2 kyr event. It is therefore likely that these long-term changes are more influenced by local summer insolation than by an Atlantic climatic anomaly, as suggested by Kilhavn et al. (2022). Thus, other stalagmite records from the region (Kilhavn et al., 2022) and the combination of the carbon isotopic composition ($\delta^{18}O_c$ and $\delta^{13}C_c$) and the FI record from Mendukilo stalagmites offers a better understanding of the regional response during this colder-than-average Holocene period, which was characterized by increased humidity and changes in moisture source composition (Domínguez-Villar et al., 2009; Kilhavn et al., 2022; Bernal-Wormull et al., 2023).

6. CONCLUSIONS

The Ostolo and Mendukilo speleothems provide a replicated and precisely dated record of paleotemperature in NE Iberia for the past 16.5 kyr BP. The OM-FIT record contributes novel, non-biogenic evidence of rapid temperature transitions during the last deglaciation and the Holocene, including the identification of abrupt events. Our findings indicate temperatures for GS-2.1a up to 6.0 ± 1.9 °C lower than those for GI-1 and present-day conditions, and constrain the regional response of HE-1 between 16.2 and 15.8 kyr BP. The sharp rise in temperatures during the GS-2.1a/GI-1 transition was quantitatively comparable to other records from SW Europe. Temperatures during GI-1 were equivalent to those of the Holocene, with a minimum observed at 14.1 ± 0.1 kyr BP during GI-1d. The rapid temperature changes at early GS-1 and the onset of the Holocene recorded by OM-FIT are consistent with to those reported from other parts of Europe. Neither $\delta^{18}O_c$ nor OM-FIT reveal significant millennial-scale changes during the Holocene. The 8.2 kyr event is recorded between 8.29 and 8.10 ± 0.04 kyr in the $\delta^{18}O_c$ record, centered at 8.29 ± 0.07 kyr in the OM-FIT record, synchronous with Greenland ice-core data and well-dated records from central and southwestern Europe.

https://doi.org/10.5194/egusphere-2024-3612
Preprint. Discussion started: 26 November 2024

Appendix A

Table A1. FI δ^2H measurements of Ostolo samples. The δ^2H values were corrected for the ice-volume effect during the deglaciation period covered by the Ostolo speleothems. Each time span of each sample represents the duration covered by the respective calcite blocks sampled from the stalagmites used for the fluid inclusion measurements (without taking into account the age model uncertainty).

FI sample	Water amount (μL)	Water content (μL/g)	δ^2H (‰ VSMOW) measured	Mean δ^2H (‰ VSMOW)	δ^2H Std Dev	δ^2H Error	Mean δ^2H adjusted for IV (‰ VSMOW)	Age (kyr BP)
OST1-16.1A	0.52	0.27	-50.85	-49.74	1.57	2.70	-57.08	16.06 ± 0.06
OST1-16.1B	0.69	0.45	-48.62					
OST1-15.2A	0.04	0.06	-54.99	-51.43	3.38	3.38	-57.98	15.16 ± 0.05
OST1-15.2B	0.18	0.18	-51.05					
OST1-15.2C	0.87	0.31	-48.26					
OST1-14.6A	0.39	0.39	-25.99	-25.37	0.88	2.70	-31.36	14.57 ± 0.05
OST1-14.6B	0.86	0.79	-24.75					
OST1-14.2A	0.11	0.44	-43.68	-43.39	0.41	2.70	-49.09	14.20 ± 0.02
OST1-14.2B	0.10	0.29	-43.10					
OST1-13.0	0.57	0.37	-32.51	-32.51	n/a	2.70	-36.96	13.02 ± 0.04
OST1-10.9A	0.19	0.17	-29.28	-26.58	3.82	3.82	-28.86	10.95 ± 0.20
OST1-10.9B	0.12	0.40	-23.87					
OST3-16.4	0.11	0.37	-46.07	-46.07	n/a	2.70	-53.59	16.40 ± 0.11
OST3-14.3	0.21	0.18	-26.03	-26.03	n/a	2.70	-31.83	14.30 ± 0.09
OST3-14.1A	0.09	0.07	-36.69	-35.29	1.62	2.70	-40.89	14.11 ± 0.09
OST3-14.1B	0.19	0.13	-33.52					
OST3-14.1C	0.20	0.19	-35.66					
OST3-13.5A	0.14	0.13	-34.48	-34.91	2.15	2.70	-39.90	13.50 ± 0.09
OST3-13.5B	0.18	0.14	-33.01					
OST3-13.5C	0.16	0.11	-37.25					
OST3-13.0	0.20	0.14	-30.97	-30.97	n/a	2.70	-35.43	13.00 ± 0.08
OST3-12.9	0.12	0.12	-42.50	-42.50	n/a	2.70	-46.85	12.90 ± 0.06
OST3-12.8	0.17	0.14	-43.75	-43.75	n/a	2.70	-47.98	12.80 ± 0.08
OST3-11.7A	0.11	0.12	-26.15	-24.99	1.64	2.70	-27.92	11.67 ± 0.02
OST3-11.7B	0.24	0.27	-23.83					
OST3-11.6A	0.09	0.08	-35.16	-39.68	6.39	6.39	-42.60	11.60 ± 0.02
OST3-11.6B	0.14	0.15	-44.19					
OST3-11.5A	0.28	0.25	-31.94	-32.76	1.16	2.70	-35.58	11.49 ± 0.01
OST3-11.5B	0.32	0.24	-33.58					
OST3-11.3A	0.12	0.14	-39.55	-40.01	0.64	2.70	-42.63	11.30 ± 0.02
OST3-11.3B	0.15	0.11	-40.46					

https://doi.org/10.5194/egusphere-2024-3612
Preprint. Discussion started: 26 November 2024

Table A1. Continued

FI sample	Water amount (µL)	Water content (µL/g)	δ²H (‰ VSMOW) measured	Mean δ²H (‰ VSMOW)	δ²H Std Dev	δ²H Error	Mean δ²H adjusted for IV (‰ VSMOW)	Age (kyr BP)
OST2-16.7	0.11	0.37	-46.07	-46.07	n/a	2.70	-57.13	16.70 ± 0.07
OST2-16.4A	0.34	0.31	-52.39	-49.76	2.69	2.70	-57.29	16.40 ± 0.05
OST2-16.4B	0.27	0.23	-47.00					
OST2-16.4C	0.39	0.90	-49.89					
OST2-15.8A	0.10	0.12	-57.86	-59.72	2.63	2.70	-66.84	15.80 ± 0.07
OST2-15.8B	0.09	0.08	-61.57					
OST2-15.3	0.33	0.17	-46.78	-46.78	n/a	2.40	-53.50	15.31 ± 0.08
OST2-14.7	0.18	0.14	-38.53	-38.53	n/a	2.40	-44.71	14.71 ± 0.18
OST2-14.0A	0.10	0.15	-54.96	-50.45	6.39	6.39	-56.05	14.10 ± 0.09
OST2-14.0B	0.10	0.09	-45.93					
OST2-13.0A	0.38	0.51	-23.17	-26.035	3.32	3.32	-30.49	13.00 ± 0.08
OST2-13.0B	0.72	0.94	-23.27					
OST2-13.0C	0.47	0.61	-28.04					
OST2-13.0D	0.40	0.44	-29.66					
OST2-12.9A	0.08	0.14	-40.16	-40.85	0.97	2.70	-45.19	12.89 ± 0.07
OST2-12.9B	0.09	0.15	-41.54					
OST2-12.5A	0.09	0.11	-50.51	-50.865	0.50	2.70	-54.74	12.50 ± 0.10
OST2-12.5B	0.11	0.12	-51.22					
OST2-12.3A	0.23	0.32	-45.28	-50.125	6.85	6.85	-53.69	12.29 ± 0.10
OST2-12.3B	0.19	0.23	-54.97					
OST2-11.8	0.16	0.11	-44.45	-44.45	n/a	2.70	-47.59	11.80 ± 0.03
OST2-11.65A	0.25	0.17	-38.01	-36.705	1.84	2.70	-39.74	11.65 ± 0.02
OST2-11.65B	0.43	0.23	-35.40					
OST2-11.5A	0.18	0.12	-28.62	-28.675	0.07	2.70	-31.50	11.50 ± 0.01
OST2-11.5B	0.22	0.41	-28.73					
OST2-10.9A	0.09	0.24	-44.38	-39.605	6.75	6.75	-41.89	10.90 ± 0.08
OST2-10.9B	0.22	0.38	-34.83					

https://doi.org/10.5194/egusphere-2024-3612
Preprint. Discussion started: 26 November 2024

Table A2. FI δ^{2}H measurements of Mendukilo samples. The δ^{2}H values were corrected for the ice-volume effect during the period covered by the Mendukilo speleothems. Each time span of each sample represents the duration covered by the respective calcite blocks sampled from the stalagmites used for the fluid inclusion measurements (without taking into account the age model uncertainty).

FI sample	Water amount (μL)	Water content (μL/g)	δ^{2}H (‰ VSMOW) measured	Mean δ^{2}H (‰ VSMOW)	δ^{2}H Std Dev	δ^{2}H Error	Mean δ^{2}H adjusted for IV (‰ VSMOW)	Age (kyr BP)
Men2-botA	0.61	0.29	-37.67	-40.40	2.91	2.91	-44.85	12.90 ± 0.10
Men2-botB	0.54	0.33	-37.62					
Men2-botC	0.18	0.11	-44.43					
Men2-botD	0.28	0.21	-40.35					
Men2-botE	0.30	0.18	-41.94					
Men2-0A	0.18	0.19	-48.93	-47.75	1.24	2.70	-51.98	12.78 ± 0.10
Men2-0B	0.32	0.21	-47.88					
Men2-0C	0.30	0.29	-46.44					
Men2-5A	0.16	0.27	-55.39	-57.33	2.74	2.74	-61.31	12.65 ± 0.10
Men2-5B	0.14	0.13	-59.26					
Men2-10A	0.33	0.20	-47.04	-48.12	1.53	2.70	-52.00	12.51 ± 0.10
Men2-10B	0.12	0.11	-49.20					
Men2-17A	0.07	0.08	-46.23	-47.74	3.81	3.81	-51.40	12.32 ± 0.10
Men2-17B	0.21	0.19	-52.85					
Men2-17C	0.07	0.09	-48.00					
Men2-17D	0.35	0.21	-43.86					
Men2-22A	0.13	0.11	-44.45	-46.58	4.14	4.14	-50.14	12.21 ± 0.10
Men2-22B	0.15	0.11	-51.36					
Men2-22C	0.23	0.12	-43.93					
Men2-27A	0.22	0.22	-46.64	-48.10	1.89	2.70	-51.45	12.08 ± 0.10
Men2-27B	0.26	0.29	-47.66					
Men2-27C	0.22	0.22	-50.87					
Men2-27D	0.12	0.10	-47.24					
Men2-35A	0.71	0.62	-43.10	-45.31	1.89	2.70	-48.45	11.83 ± 0.10
Men2-35B	0.40	0.29	-45.77					
Men2-35C	0.62	0.55	-44.76					
Men2-35D	0.16	0.14	-47.62					
Men2-43A	0.15	0.15	-46.48	-44.28	3.83	3.83	-47.10	11.59 ± 0.08
Men2-43B	0.23	0.26	-38.55					
Men2-43C	0.14	0.15	-46.28					
Men2-43D	0.14	0.18	-45.79					
Men2-47A	0.25	0.36	-48.00	-50.72	2.35	2.70	-53.54	11.50 ± 0.08
Men2-47B	0.26	0.36	-52.12					
Men2-47C	0.13	0.18	-52.03					
Men2-48A	0.15	0.17	-35.09	-33.49	2.26	2.70	-36.32	11.48 ± 0.08
Men2-48B	0.51	0.59	-31.89					

https://doi.org/10.5194/egusphere-2024-3612
Preprint. Discussion started: 26 November 2024

Table A2. Continued

FI sample	Water amount (μL)	Water content (μL/g)	δ^2H (‰ VSMOW) measured	Mean δ^2H (‰ VSMOW)	δ^2H Std Dev	δ^2H Error	Mean δ^2H adjusted for IV (‰ VSMOW)	Age (kyr BP)
Men2-52A	0.18	0.22	-38.95					
Men2-52B	0.13	0.18	-40.61	-40.49	1.49	2.70	-43.22	11.37 ± 0.08
Men2-52C	0.67	0.64	-41.92					
Men2-62A	0.46	0.74	-43.51					
Men2-62B	0.30	0.44	-36.89	-39.55	3.23	3.23	-42.09	11.20 ± 0.08
Men2-62C	0.30	0.63	-36.94					
Men2-62D	0.10	0.12	-40.85					
Men2-73A	0.18	0.21	-35.37	-35.15	0.31	2.70	-37.52	11.01 ± 0.06
Men2-73B	0.68	0.76	-34.93					
Men2-78A	0.23	0.25	-43.7					
Men2-78B	0.10	0.18	-40.88	-43.58	2.64	2.70	-45.86	10.93 ± 0.06
Men2-78C	0.16	0.17	-46.16					
Men2-85A	0.16	0.21	-46.25					
Men2-85B	0.27	0.26	-48.37	-46.39	1.90	2.70	-48.59	10.81 ± 0.06
Men2-85C	0.18	0.19	-44.56					
Men2-92A	0.32	0.3	-35.24					
Men2-92B	0.21	0.22	-38.56	-37.76	2.23	2.70	-39.88	10.69 ± 0.06
Men2-92C	0.20	0.25	-39.48					
Men2-97A	0.26	0.29	-43.22					
Men2-97B	0.18	0.21	-41.79	-43.25	1.48	2.70	-45.3	10.60 ± 0.06
Men2-97C	0.14	0.12	-44.75					
Men2-108A	0.13	0.13	-36.06	-37.03	1.37	2.70	-38.95	10.41 ± 0.06
Men2-108B	0.35	0.38	-38					
Men2-116A	0.14	0.17	-46.21					
Men2-116B	0.33	0.35	-38.84	-42.83	3.72	3.72	-44.69	10.28 ± 0.06
Men2-116C	0.17	0.14	-43.45					
Men2-122A	0.24	0.3	-49.32					
Men2-122B	0.12	0.14	-45.04	-46.42	2.51	2.70	-48.17	10.07 ± 0.06
Men2-122C	0.55	0.48	-44.89					
Men2-128A	0.15	0.17	-31.97					
Men2-128B	0.12	0.14	-29.34	-32.91	4.11	4.11	-34.56	9.96 ± 0.08
Men2-128C	0.44	0.41	-37.41					
Men2-134A	0.32	0.33	-41.27					
Men2-134B	0.39	0.46	-39.7	-40.59	0.80	2.70	-42.18	9.84 ± 0.08
Men2-134C	0.25	0.18	-40.79					
Men2-155A	0.66	0.61	-37.15					
Men2-155B	0.35	0.34	-32.35	-38.19	6.42	6.42	-39.57	9.43 ± 0.08
Men2-155C	0.39	0.36	-45.06					
Men2-162A	0.19	0.15	-53.89					
Men2-162B	0.21	0.16	-47.28	-49.26	3.16	3.16	-50.59	9.29 ± 0.08
Men2-162C	0.11	0.13	-47.23					
Men2-162D	0.21	0.13	-48.63					

https://doi.org/10.5194/egusphere-2024-3612
Preprint. Discussion started: 26 November 2024

Table A2. Continued

FI sample	Water amount (μL)	Water content (μL/g)	δ^2H (‰ VSMOW) measured	Mean δ^2H (‰ VSMOW)	δ^2H Std Dev	δ^2H Error	Mean δ^2H adjusted for IV (‰ VSMOW)	Age (kyr BP)
Men2-177A	0.33	0.32	-39.30	-39.17	0.18	2.70	-40.38	9.01 ± 0.08
Men2-177B	0.35	0.23	-39.05					
Men2-185A	0.10	0.10	-44.21	-44.13	3.42	3.42	-45.25	8.85 ± 0.08
Men2-185B	0.19	0.10	-47.50					
Men2-185C	0.21	0.12	-40.67					
Men2-192A	0.14	0.16	-42.95	-38.32	4.25	4.25	-39.41	8.72 ± 0.08
Men2-192B	0.17	0.16	-34.61					
Men2-192C	0.38	0.19	-37.39					
Men2-200A	0.38	0.35	-40.42	-42.33	1.69	2.70	-43.35	8.57 ± 0.08
Men2-200B	0.37	0.24	-42.93					
Men2-200C	0.22	0.17	-43.63					
Men2-207A	0.11	0.09	-43.67	-43.23	0.62	2.70	-44.23	8.43 ± 0.08
Men2-207B	0.19	0.15	-42.79					
Men2-215A	0.15	0.12	-48.65	-52.55	3.96	3.96	-53.51	8.28 ± 0.08
Men2-215B	0.18	0.14	-56.10					
Men2-215C	0.25	0.15	-55.81					
Men2-215D	0.25	0.18	-49.63					
Men2-251A	0.23	0.16	-42.11	-39.36	2.39	2.70	-40.15	7.54 ± 0.08
Men2-251B	0.46	0.35	-38.20					
Men2-251C	0.17	0.09	-37.78					
Men2-267A	0.13	0.12	-43.70	-49.38	4.04	4.04	-50.11	7.20 ± 0.08
Men2-267B	0.16	0.10	-52.75					
Men2-267C	0.16	0.10	-51.67					
Men2-267D	0.20	0.13	-49.38					
Men2-282A	0.15	0.11	-44.16	-45.59	1.72	2.70	-46.27	6.88 ± 0.08
Men2-282B	0.38	0.27	-45.10					
Men2-282C	0.20	0.11	-47.50					
Men2-295A	0.19	0.15	-47.52	-46.54	3.14	3.14	-47.18	6.59 ± 0.08
Men2-295B	0.22	0.21	-42.13					
Men2-295C	0.16	0.12	-46.96					
Men2-295D	0.17	0.13	-49.54					
Men2-301A	0.11	0.08	-49.69	-49.93	1.25	2.70	-50.53	6.47 ± 0.08
Men2-301B	0.21	0.14	-48.81					
Men2-301C	0.14	0.08	-51.28					
Men2-307A	0.08	0.05	-43.49	-44.21	1.84	2.70	-44.8	6.34 ± 0.08
Men2-307B	0.16	0.11	-46.3					
Men2-307C	0.16	0.11	-42.84					
Men2-310A	0.20	0.18	-49.79	-46.10	5.06	5.06	-46.69	6.28 ± 0.08
Men2-310B	0.25	0.21	-40.32					
Men2-310C	0.18	0.12	-48.18					
Men2-312A	0.38	0.25	-45.11	-44.22	0.83	2.70	-44.79	6.20 ± 0.08
Men2-312B	0.52	0.35	-44.08					
Men2-312C	0.33	0.34	-43.46					

https://doi.org/10.5194/egusphere-2024-3612
Preprint. Discussion started: 26 November 2024

Table A2. Continued

FI sample	Water amount (µL)	Water content (µL/g)	δ^2H (‰ VSMOW) measured	Mean δ^2H (‰ VSMOW)	δ^2H Std Dev	δ^2H Error	Mean δ^2H adjusted for IV (‰ VSMOW)	Age (kyr BP)
Men5-10A	0.82	0.94	-41.84					
Men5-10B	0.19	0.34	-36.02	-38.74	2.93	2.93	-39.84	8.72 ± 0.06
Men5-10C	0.19	0.19	-38.37					
Men5-20A	0.23	0.24	-40.05					
Men5-20B	0.28	0.26	-41.18	-39.75	1.60	2.70	-40.81	8.58 ± 0.06
Men5-20C	0.21	0.19	-38.02					
Men5-30A	0.15	0.16	-44.41					
Men5-30B	0.44	0.34	-37.73	-40.39	3.54	3.54	-41.38	8.45 ± 0.06
Men5-30C	0.24	0.18	-39.02					
Men5-40A	0.39	0.35	-48.60					
Men5-40B	0.11	0.10	-61.67	-55.29	6.54	6.54	-56.26	8.31 ± 0.06
Men5-40C	0.11	0.10	-55.61					
Men5-50A	0.23	0.20	-37.79					
Men5-50B	0.50	0.50	-42.30	-39.76	2.31	2.70	-40.68	8.17 ± 0.06
Men5-50C	0.34	0.36	-39.20					
Men5-60A	0.30	0.25	-42.78					
Men5-60B	0.49	0.40	-47.14	-43.98	2.76	2.76	-44.87	8.04 ± 0.06
Men5-60C	0.20	0.18	-42.03					
Men5-70A	0.14	0.16	-39.45					
Men5-70B	0.29	0.29	-43.86	-42.62	3.91	3.91	-43.483	7.90 ± 0.06
Men5-70C	0.09	0.11	-47.60					
Men5-70D	0.20	0.16	-39.55					
Men5-75A	0.16	0.16	-50.84					
Men5-75B	0.24	0.24	-48.46	-49.47	1.23	2.70	-50.31	7.84 ± 0.06
Men5-75C	0.27	0.27	-49.10					
Men5-80A	0.18	0.18	-33.70					
Men5-80B	0.33	0.30	-37.03	-37.37	3.84	3.84	-38.21	7.77 ± 0.06
Men5-80C	0.23	0.21	-41.37					
Men5-90A	0.22	0.24	-41.35					
Men5-90B	0.20	0.19	-48.91	-43.97	4.49	4.49	-44.77	7.63 ± 0.06
Men5-90C	0.12	0.19	-46.44					
Men5-90D	0.29	0.23	-39.16					
Men5-100A	0.12	0.14	-37.33					
Men5-100B	0.10	0.14	-45.66	-40.53	4.49	4.49	-41.31	7.50 ± 0.06
Men5-100C	0.21	0.16	-38.59					
Men5-110A	0.25	0.22	-40.90					
Men5-110B	0.20	0.17	-33.13	-36.39	4.03	4.03	-37.16	7.37 ± 0.06
Men5-110C	0.56	0.44	-35.13					
Men5-120A	0.21	0.21	-42.86					
Men5-120B	0.63	0.73	-44.84	-44.00	1.08	2.7	-44.74	7.23 ± 0.06
Men5-120C	0.73	0.87	-43.29					
Men5-120D	0.32	0.55	-45.01					

https://doi.org/10.5194/egusphere-2024-3612
Preprint. Discussion started: 26 November 2024

Table A2. Continued

FI sample	Water amount (μL)	Water content (μL/g)	δ^2H (‰ VSMOW) measured	Mean δ^2H (‰ VSMOW)	δ^2H Std Dev	δ^2H Error	Mean δ^2H adjusted for IV (‰ VSMOW)	Age (kyr BP)
Men5-130A	0.19	0.16	-42.10					
Men5-130B	0.34	0.27	-47.22	-43.79	2.97	2.97	-44.51	7.08 ± 0.06
Men5-130C	0.21	0.22	-42.05					
Men5-140A	0.18	0.23	-49.92	-48.32	2.26	2.7	-49.01	6.93 ± 0.06
Men5-140B	0.20	0.23	-46.72					
Men5-150A	0.26	0.26	-42.23					
Men5-150B	0.30	0.23	-46.99	-43.88	2.70	2.70	-44.53	6.75 ± 0.06
Men5-150C	0.21	0.19	-42.41					
Men5-160A	0.35	0.32	-40.50					
Men5-160B	0.47	0.39	-45.46	-42.37	2.69	2.70	-43.01	6.58 ± 0.06
Men5-160C	0.30	0.21	-41.16					
Men5-170A	0.22	0.22	-34.99					
Men5-170B	0.27	0.27	-37.43	-38.44	2.85	2.85	-39.04866731	6.45 ± 0.06
Men5-170C	0.20	0.41	-39.83					
Men5-170D	0.19	0.14	-41.52					
Men5-180A	0.39	0.3	-44.03					
Men5-180B	0.3	0.3	-40.73	-42.33	1.65	2.70	-42.92	6.31 ± 0.08
Men5-180C	0.45	0.34	-42.22					
Men5-190A	0.21	0.19	-36.51	-37.98	2.08	2.7	-38.5376	6.11 ± 0.08
Men5-190B	0.28	0.21	-39.45					
Men5-200A	0.19	0.17	-47.17					
Men5-200B	0.17	0.14	-46.04	-43.85	4.81	4.81	-44.37	5.92 ± 0.08
Men5-200C	0.30	0.22	-38.34					
Men5-210A	0.49	0.45	-36.94					
Men5-210B	0.29	0.27	-42.43	-38.92	3.05	3.05	-39.40	5.72 ± 0.08
Men5-210C	0.36	0.3	-37.38					
Men5-220A	0.34	0.68	-39.84					
Men5-220B	0.32	0.45	-46.05	-44.70	4.34	4.34	-45.15	5.51 ± 0.08
Men5-220C	0.24	0.32	-48.21					
Men5-230A	0.78	0.65	-36.00					
Men5-230B	0.39	0.39	-37.48	-39.08	3.26	3.26	-39.4999	5.31 ± 0.08
Men5-230C	0.26	0.42	-39.30					
Men5-230D	0.18	0.20	-43.53					
Men5-240A	0.28	0.23	-45.74					
Men5-240B	0.12	0.12	-45.76	-46.09	2.82	2.82	-46.4852	5.11 ± 0.08
Men5-240C	0.08	0.13	-43.00					
Men5-240D	0.19	0.32	-49.86					
Men5-250A	0.15	0.14	-42.27					
Men5-250B	0.17	0.15	-37.67	-39.25	2.62	2.70	-39.62	4.90 ± 0.08
Men5-250C	0.36	0.51	-37.8					
Men5-260A	0.32	0.29	-44.55	-43.7	1.20	2.7	-44.052	4.70 ± 0.08
Men5-260B	0.27	0.25	-42.85					

https://doi.org/10.5194/egusphere-2024-3612
Preprint. Discussion started: 26 November 2024

Table A2. Continued

FI sample	Water amount (μL)	Water content (μL/g)	δ^2H (‰ VSMOW) measured	Mean δ^2H (‰ VSMOW)	δ^2H Std Dev	δ^2H Error	Mean δ^2H adjusted for IV (‰ VSMOW)	Age (kyr BP)
Men5-280A	0.3	0.49	-48.24	-48.94	0.98	2.7	-49.2582	4.29 ± 0.08
Men5-280B	0.39	0.66	-49.63					
Men5-290A	0.26	0.21	-46.14	-45.31	3.15	3.15	-45.62	4.08 ± 0.08
Men5-290B	0.15	0.13	-47.96					
Men5-290C	0.34	0.30	-41.83					
Men5-300A	0.19	0.17	-40.54	-38.64	1.93	2.70	-38.93	3.88 ± 0.08
Men5-300B	0.20	0.16	-36.69					
Men5-300C	0.46	0.46	-38.68					
Men5-310A	0.32	0.27	-44.06	-43.78	1.10	2.70	-44.06	3.67 ± 0.08
Men5-310B	0.23	0.20	-42.56					
Men5-310C	0.40	0.32	-44.71					
Men5-330A	0.18	0.14	-39.60	-41.31	3.80	3.80	-41.56	3.26 ± 0.08
Men5-330B	0.75	0.51	-45.67					
Men5-330C	0.31	0.52	-38.65					
Men5-340A	0.21	0.17	-40.10	-44.00	3.40	3.40	-44.23	3.06 ± 0.08
Men5-340B	0.51	0.51	-46.30					
Men5-340C	0.77	0.72	-45.60					
Men5-350A	0.34	0.31	-40.68	-41.63	2.88	2.88	-41.85	2.85 ± 0.08
Men5-350B	0.14	0.17	-44.87					
Men5-350C	0.26	0.24	-39.35					
Men5-360A	0.24	0.19	-40.35	-37.63	3.10	3.10	-37.84	2.65 ± 0.08
Men5-360B	0.25	0.22	-34.25					
Men5-360C	0.47	0.38	-38.28					
Men5-380A	0.29	0.24	-37.38	-37.11	1.7	2.7	-37.3101276	2.37 ± 0.06
Men5-380B	0.18	0.16	-34.88					
Men5-380C	0.42	0.50	-39.02					
Men5-380D	0.28	0.24	-37.16					
Men5-390A	0.45	0.40	-40.75	-47.66	4.91	4.91	-47.843	2.25 ± 0.04
Men5-390B	0.21	0.27	-48.49					
Men5-390C	0.15	0.16	-52.38					
Men5-390D	0.15	0.12	-49.00					
Men5-430A	0.20	0.20	-37.13	-34.01	3.05	3.05	-34.18	1.84 ± 0.04
Men5-430B	0.25	0.19	-33.86					
Men5-430C	0.43	0.43	-31.03					
Men5-440A	0.30	0.25	-32.55	-35.98	3.36	3.36	-36.14	1.73 ± 0.04
Men5-440B	0.26	0.20	-36.12					
Men5-440C	0.45	0.37	-39.27					
Men5-450A	0.13	0.21	-46.89	-46.48	0.58	2.7	-46.6384	1.63 ± 0.04
Men5-450B	0.21	0.24	-46.07					
Men5-460A	0.39	0.34	-39.2	-38.00	2.28	2.70	-38.15	1.53 ± 0.04
Men5-460B	0.15	0.15	-35.37					
Men5-460C	0.50	0.40	-39.42					

https://doi.org/10.5194/egusphere-2024-3612
Preprint. Discussion started: 26 November 2024

Table A2. Continued

FI sample	Water amount (μL)	Water content (μL/g)	δ^2H (‰ VSMOW) measured	Mean δ^2H (‰ VSMOW)	δ^2H Std Dev	δ^2H Error	Mean δ^2H adjusted for IV (‰ VSMOW)	Age (kyr BP)
Men5-470A	0.34	0.31	-35.32					
Men5-470B	0.47	0.56	-40.48	-39.58	3.88	3.88	-39.73	1.43 ± 0.04
Men5-470C	0.16	0.17	-42.93					
Men5-480A	0.26	0.29	-44.99					
Men5-480B	0.19	0.21	-37.38	-41.20	3.81	3.81	-41.35	1.34 ± 0.04
Men5-480C	0.14	0.12	-41.24					
Men5-490A	0.18	0.13	-40.52					
Men5-490B	0.21	0.17	-43.44	-41.50	1.68	2.70	-41.64	1.24 ± 0.04
Men5-490C	0.38	0.32	-40.54					
Men5-505A	0.33	0.29	-34.40					
Men5-505B	0.15	0.13	-35.35	-35.45	1.11	2.70	-35.59	1.10 ± 0.04
Men5-505C	0.14	0.12	-36.61					
Men5-515A	0.18	0.15	-43.39					
Men5-515B	0.14	0.12	-49.37	-46.27	3.00	3.00	-46.40	0.99 ± 0.04
Men5-515C	0.26	0.20	-46.04					
Men5-525A	0.21	0.20	-36.35					
Men5-525B	0.21	0.19	-36.79	-38.42	3.21	3.21	-38.55	0.90 ± 0.04
Men5-525C	0.48	0.39	-42.11					
Men5-540A	0.22	0.19	-43.04					
Men5-540B	0.29	0.25	-46.74	-44.97	1.86	2.70	-45.09	0.75 ± 0.04
Men5-540C	0.18	0.13	-45.13					
Men5-550A	0.16	0.15	-46.65					
Men5-550B	0.41	0.39	-44.63	-46.36	1.60	2.70	-46.48	0.65 ± 0.04
Men5-550C	0.18	0.20	-47.79					
Men5-560A	0.36	0.37	-42.81					
Men5-560B	0.22	0.23	-44.28	-45.39	3.28	3.28	-45.51	0.55 ± 0.04
Men5-560C	0.29	0.26	-49.08					
Men5-570A	0.56	0.45	-44.35					
Men5-570B	0.57	0.43	-39.72	-43.13	3.00	3.00	-43.25	0.45 ± 0.04
Men5-570C	0.43	0.37	-45.33					
Men5-580A	0.53	0.46	-41.65					
Men5-580B	0.47	0.50	-45.46	-43.02	2.12	2.70	-43.13	0.35 ± 0.04
Men5-580C	0.48	0.45	-41.95					
Men5-590A	0.15	0.13	-50.41					
Men5-590B	0.17	0.15	-46.03	-46.88	3.19	3.19	-46.99	0.25 ± 0.04
Men5-590C	0.56	0.59	-44.20					
Men5-600A	0.26	0.27	-47.86					
Men5-600B	0.45	0.54	-41.08	-43.66	3.67	3.67	-43.77	0.15 ± 0.04
Men5-600C	0.54	0.47	-42.05					

https://doi.org/10.5194/egusphere-2024-3612
Preprint. Discussion started: 26 November 2024

Table A3. Paleotemperatures obtained from δ^2H_{FI} data using the OM-FIT transfer function.

Sample (stratigraphic order)	Age (kyr BP)	Mean δ^2H adjusted for IV (‰ VSMOW)	δ^2H corrected error ± (‰)	Temp. (°C) OM-FIT	Error ± (°C)
OST2-16.7	16.70 ± 0.07	-57.13	2.70	8.14	2.05
OST2-16.4	16.40 ± 0.05	-57.29	2.70	8.11	2.05
OST1-16.1	16.06 ± 0.06	-57.08	2.70	8.15	2.05
OST2-15.8	15.80 ± 0.07	-66.84	2.70	5.94	2.05
OST2-15.3	15.31 ± 0.08	-53.5	2.70	8.97	2.05
OST1-15.2	15.16 ± 0.05	-57.98	3.38	7.95	2.07
OST2-14.7	14.78 ± 0.18	-44.71	2.70	10.97	2.05
OST1-14.6	14.57 ± 0.05	-31.36	2.70	14.00	2.05
OST3-14.3	14.30 ± 0.09	-31.83	2.70	13.89	2.05
OST1-14.2	14.20 ± 0.02	-49.09	2.70	9.97	2.05
OST3-14.1	14.11 ± 0.09	-40.89	2.70	11.83	2.05
OST2-14.0	14.10 ± 0.09	-56.05	6.39	8.39	2.89
OST3-13.5	13.50 ± 0.09	-39.90	2.70	12.06	2.05
OST2-13.0	13.00 ± 0.08	-30.49	3.32	14.20	2.19
Men2-bot	12.90 ± 0.10	-44.85	2.91	11.72	1.76
OST2-12.9	12.89 ± 0.07	-45.19	2.70	10.86	2.05
OST3-12.8	12.80 ± 0.08	-47.98	2.70	10.22	2.05
Men2-0	12.78 ± 0.10	-51.98	2.70	10.11	1.76
Men2-5	12.65 ± 0.10	-61.31	2.74	7.98	1.77
Men2-10	12.51 ± 0.10	-52.00	2.70	10.10	1.76
OST2-12.5	12.50 ± 0.10	-54.74	2.70	8.69	2.05
Men2-17	12.32 ± 0.10	-51.40	3.81	10.24	2.02
OST2-12.3	12.29 ± 0.10	-53.69	6.85	8.93	3.00
Men2-22	12.21 ± 0.10	-50.14	4.14	10.52	2.09
Men2-27	12.08 ± 0.10	-51.45	2.70	10.22	1.76
Men2-35	11.83 ± 0.10	-48.45	2.70	10.91	1.76
OST2-11.8	11.80 ± 0.03	-47.59	2.70	10.31	2.05
OST3-11.7	11.67 ± 0.02	-27.92	2.70	14.78	2.05
OST2-11.65	11.65 ± 0.02	-39.74	2.70	12.10	2.05
OST3-11.6	11.60 ± 0.02	-42.6	6.39	11.45	2.89
Men2-43	11.59 ± 0.08	-47.10	3.83	11.21	2.02
Men2-47	11.50 ± 0.08	-53.54	2.70	9.75	1.76
OST2-11.5	11.50 ± 0.01	-31.5	2.70	13.97	2.05
Men2-48	11.48 ± 0.08	-36.32	2.70	13.66	1.76
Men2-52	11.37 ± 0.08	-43.22	2.70	12.10	1.76
OST3-11.3	11.30 ± 0.02	-42.63	2.70	11.44	2.05
Men2-62	11.20 ± 0.08	-42.09	3.23	12.35	1.88
Men2-73	11.01 ± 0.06	-37.52	2.70	13.39	1.76
OST1-10.9	10.95 ± 0.20	-28.86	3.82	14.57	2.31
Men2-78	10.93 ± 0.06	-45.86	2.70	11.50	1.75

https://doi.org/10.5194/egusphere-2024-3612
Preprint. Discussion started: 26 November 2024

Table A3. Continued

OST2-10.9	10.90 ± 0.08	-41.89	6.75	11.61	2.97
Men2-85	10.81 ± 0.06	-48.59	2.70	10.87	1.76
Men2-92	10.69 ± 0.06	-39.88	2.70	12.85	1.76
Men2-97	10.60 ± 0.06	-45.30	2.70	11.62	1.76
Men2-108	10.41 ± 0.06	-38.95	2.70	13.07	1.76
Men2-116	10.28 ± 0.06	-44.69	3.72	11.76	2.00
Men2-122	10.07 ± 0.06	-48.17	2.70	10.97	1.76
Men2-128	9.96 ± 0.08	-34.56	4.11	14.06	2.09
Men2-134	9.84 ± 0.08	-42.18	2.70	12.33	1.76
Men2-155	9.43 ± 0.08	-39.57	6.42	12.92	2.61
Men2-162	9.29 ± 0.08	-50.59	3.16	10.42	1.87
Men2-177	9.01 ± 0.08	-40.38	2.70	12.74	1.76
Men2-185	8.85 ± 0.08	-45.25	3.42	11.63	1.93
Men5-10	8.72 ± 0.06	-39.84	2.93	12.86	1.82
Men5-20	8.58 ± 0.06	-40.81	2.70	12.64	1.76
Men2-200	8.57 ± 0.08	-43.35	2.70	12.07	1.76
Men5-30	8.45 ± 0.06	-41.38	3.54	12.51	1.96
Men2-207	8.43 ± 0.08	-44.23	2.70	11.87	1.76
Men5-40	8.31 ± 0.06	-56.26	6.54	9.13	2.64
Men2-215	8.28 ± 0.08	-53.51	3.96	9.76	2.05
Men5-50	8.17 ± 0.06	-40.68	2.70	12.67	1.76
Men5-60	8.04 ± 0.06	-44.87	2.76	11.72	1.78
Men5-70	7.90 ± 0.06	-43.48	3.91	12.04	2.04
Men5-75	7.84 ± 0.06	-50.31	2.70	10.48	1.76
Men5-80	7.77 ± 0.06	-38.21	3.84	13.23	2.02
Men5-90	7.63 ± 0.06	-44.77	4.49	11.74	2.17
Men2-251	7.54 ± 0.08	-40.15	2.70	12.79	1.76
Men5-100	7.50 ± 0.06	-41.31	4.49	12.53	2.17
Men5-110	7.37 ± 0.06	-37.16	4.03	13.47	2.07
Men5-120	7.23 ± 0.06	-44.74	2.70	11.75	1.76
Men2-267	7.20 ± 0.08	-50.11	4.04	10.53	2.07
Men5-130	7.08 ± 0.06	-44.51	2.97	11.80	1.83
Men5-140	6.93 ± 0.06	-49.01	2.70	10.78	1.76
Men2-282	6.88 ± 0.08	-46.27	2.70	11.40	1.76
Men5-150	6.75 ± 0.06	-44.53	2.70	11.80	1.76
Men2-295	6.59 ± 0.08	-47.18	3.14	11.20	1.86
Men5-160	6.58 ± 0.06	-43.01	2.70	12.14	1.76
Men2-301	6.47 ± 0.08	-50.53	2.70	10.43	1.76
Men5-170	6.45 ± 0.06	-39.05	2.85	13.04	1.80
Men2-307	6.34 ± 0.08	-44.80	2.70	11.74	1.76
Men5-180	6.31 ± 0.08	-42.92	2.70	12.16	1.76
Men2-310	6.28 ± 0.08	-46.69	5.06	11.31	2.30
Men2-312	6.20 ± 0.08	-44.79	2.70	11.74	1.76
Men5-190	6.11 ± 0.08	-38.54	2.70	13.16	1.76
Men5-200	5.92 ± 0.08	-44.37	4.81	11.83	2.24
Men5-210	5.72 ± 0.08	-39.40	3.05	12.96	1.84
Men5-220	5.51 ± 0.08	-45.15	4.34	11.66	2.14

Table A3. Continued

Men5-230	5.31 ± 0.08	-39.50	3.26	12.94	1.89
Men5-240	5.11 ± 0.08	-46.49	2.82	11.35	1.79
Men5-250	4.90 ± 0.08	-39.62	2.70	12.91	1.76
Men5-260	4.70 ± 0.08	-44.05	2.70	11.91	1.76
Men5-280	4.29 ± 0.08	-49.26	2.70	10.72	1.76
Men5-290	4.08 ± 0.08	-45.62	3.15	11.55	1.87
Men5-300	3.88 ± 0.08	-38.93	2.70	13.07	1.76
Men5-310	3.67 ± 0.08	-44.06	2.70	11.91	1.76
Men5-330	3.26 ± 0.08	-41.56	3.80	12.47	2.02
Men5-340	3.06 ± 0.08	-44.23	3.40	11.86	1.92
Men5-350	2.85 ± 0.08	-41.85	2.88	12.41	1.80
Men5-360	2.65 ± 0.08	-37.84	3.10	13.32	1.86
Men5-380	2.37 ± 0.06	-37.31	2.70	13.44	1.76
Men5-390	2.25 ± 0.04	-47.84	4.91	11.04	2.27
Men5-430	1.84 ± 0.04	-34.18	3.05	14.15	1.84
Men5-440	1.73 ± 0.04	-36.14	3.36	13.70	1.91
Men5-450	1.63 ± 0.04	-46.64	2.70	11.32	1.76
Men5-460	1.53 ± 0.04	-38.15	2.70	13.25	1.76
Men5-470	1.43 ± 0.04	-39.73	3.88	12.89	2.03
Men5-480	1.34 ± 0.04	-41.35	3.81	12.52	2.01
Men5-490	1.24 ± 0.04	-41.64	2.70	12.45	1.76
Men5-505	1.10 ± 0.04	-35.59	2.70	13.83	1.76
Men5-515	0.99 ± 0.04	-46.40	3.00	11.37	1.83
Men5-525	0.90 ± 0.04	-38.55	3.21	13.16	1.88
Men5-540	0.75 ± 0.04	-45.09	2.70	11.67	1.76
Men5-550	0.65 ± 0.04	-46.48	2.70	11.36	1.76
Men5-560	0.55 ± 0.04	-45.51	3.28	11.58	1.90
Men5-570	0.45 ± 0.04	-43.25	3.00	12.09	1.83
Men5-580	0.35 ± 0.04	-43.13	2.70	12.12	1.76
Men5-590	0.25 ± 0.04	-46.99	3.19	11.24	1.88
Men5-600	0.15 ± 0.04	-43.77	3.67	11.97	1.98

https://doi.org/10.5194/egusphere-2024-3612
Preprint. Discussion started: 26 November 2024

DATA AVAILABILITY

The speleothem δ^{18}O data that support the findings of this study are available as a download excel file in the Supplement and all the fluid inclusion data will later be integrated in the SISAL database.

AUTHOR CONTRIBUTIONS

J.B.W, A.M., M.B., C.P.M., M.A., contributed to design this research project. J.B.W., C.S., Y.D., E.I., I.C., provided the isotopic data. J.B.W., C.P.M., L.R.E., H.C., provided the chronological data. J.B.W., A.M., E.I., provided the thin sections and/or contributed in the petrographic characterization. J.B.W., A.M., M.B., C.P.M., M.A., R.J., E.I., helped during field work. All authors contributed to the writing of the manuscript.

COMPETING INTEREST

The contact author has declared that none of the authors has any competing interests.

ACKNOWLEDGEMENTS

We are grateful to the guides and workers of the Mendukilo cave, M. Larburu and A. Govillar, for helping with the monitoring work in the cave and preserving the sampling points. We are also grateful to M. Wimmer for support during lab work at Innsbruck University, and to all people who helped during field work in the Ostolo cave (I. Altzuri and K. Sanchez). We would like to acknowledge the use of Servicio de Apoyo a la Investigacion, Zaragoza and the staff of the IsoTOPIK laboratory at University of Burgos. I. Cacho thanks the Catalan Institution for Research and Advanced Studies (ICREA) academia program from the Generalitat de Catalunya.

FINANCIAL SUPPORT

This research has been supported by the Spanish Agencia Estatal de Investigación (AEI) (grant nos. PID2019–106050RB-I00 (PYCACHU) and PID2022-139101OB-I00 (TEMPURA)). We acknowledge support of the publication fee by the CSIC Open Access Publication Support Initiative through its Unit of Information Resources for Research (URICI).

REFERENCES

Affolter, S., Fleitmann, D., and Leuenberger, M., 2014, New online method for water isotope analysis of speleothem fluid inclusions using laser absorption spectroscopy (WS-CRDS): Climate of the Past, v. 10, p. 1291–1304, doi:10.5194/cp-10-1291-2014.

Affolter, S., Häuselmann, A., Fleitmann, D., Edwards, R.L., Cheng, H., and Leuenberger, M., 2019, Central Europe temperature constrained by speleothem fluid inclusion water isotopes over the past 14,000 years: Science Advances, v. 5, p. eaav3809, doi:10.1126/sciadv.aav3809.

Allen, J.R.M., Huntley, B., and Watts, W.A., 1996, The vegetation and climate of northwest Iberia over the last 14,000 years: Journal of Quaternary Science, v. 11, p. 125–147, doi:10.1002/(SICI)1099-1417(199603/04)11:2<125::AID-JQS232>3.0.CO;2-U.

Arienzo, M.M., Swart, P.K., and Vonhof, H.B., 2013, Measurement of δ^{18}O and δ^{2}H values of fluid inclusion water in speleothems using cavity ring-down spectroscopy compared with isotope ratio mass spectrometry: Analysis of fluid inclusion water isotopes in speleothems using CRDS: Rapid Communications in Mass Spectrometry, v. 27, p. 2616–2624, doi:10.1002/rcm.6723.

Armstrong McKay, D.I., Staal, A., Abrams, J.F., Winkelmann, R., Sakschewski, B., Loriani, S., Fetzer, I., Cornell, S.E., Rockström, J., and Lenton, T.M., 2022, Exceeding 1.5°C global warming could trigger multiple climate tipping points: Science, v. 377, p. eabn7950, doi:10.1126/science.abn7950.

Baldini, L.M. et al., 2019, North Iberian temperature and rainfall seasonality over the Younger Dryas and Holocene: Quaternary Science Reviews, v. 226, p. 105998, doi:10.1016/j.quascirev.2019.105998.

Bartolomé, M., Moreno, A., Sancho, C., Stoll, H.M., Cacho, I., Spötl, C., Belmonte, Á., Edwards, R.L., Cheng, H., and Hellstrom, J.C., 2015, Hydrological change in Southern Europe responding to increasing North Atlantic overturning during Greenland Stadial 1: Proceedings of the National Academy of Sciences, v. 112, p. 6568–6572, doi:10.1073/pnas.1503990112.

Bernal-Wormull, J.L. et al., 2021, Immediate temperature response in northern Iberia to last deglacial changes in the North Atlantic: Geology, v. 49, p. 999–1003, doi:10.1130/G48660.1.

Bernal-Wormull, J.L. et al., 2023, New insights into the climate of northern Iberia during the Younger Dryas and Holocene: The Mendukilo multi-speleothem record: Quaternary Science Reviews, v. 305, p. 108006, doi:10.1016/j.quascirev.2023.108006.

Bintanja, R., van de Wal, R.S.W., and Oerlemans, J., 2005, Modelled atmospheric temperatures and global sea levels over the past million years: Nature, v. 437, p. 125–128, doi:10.1038/nature03975.

Carlson, A.E., LeGrande, A.N., Oppo, D.W., Came, R.E., Schmidt, G.A., Anslow, F.S., Licciardi, J.M., and Obbink, E.A., 2008, Rapid early Holocene deglaciation of the Laurentide ice sheet: Nature Geoscience, v. 1, p. 620–624, doi:10.1038/ngeo285.

Carrión, J.S., 2002, Patterns and processes of Late Quaternary environmental change in a montane region of southwestern Europe: Quaternary Science Reviews, v. 21, p. 2047–2066, doi:10.1016/S0277-3791(02)00010-0.

Carrión, J.S., and Van Geel, B., 1999, Fine-resolution Upper Weichselian and Holocene palynological record from Navarrés (Valencia, Spain) and a discussion about factors of Mediterranean forest succession: Review of Palaeobotany and Palynology, v. 106, p. 209–236, doi:10.1016/S0034-6667(99)00009-3.

Català, A., Cacho, I., Frigola, J., Pena, L.D., and Lirer, F., 2019, Holocene hydrography evolution in the Alboran Sea: a multi-record and multi-proxy comparison: Climate of the Past, v. 15, p. 927–942, doi:10.5194/cp-15-927-2019.

Cheng, H. et al., 2020, Timing and structure of the Younger Dryas event and its underlying climate dynamics: Proceedings of the National Academy of Sciences, v. 117, p. 23408–23417, doi:10.1073/pnas.2007869117.

Clark, P.U. et al., 2012, Global climate evolution during the last deglaciation: Proceedings of the National Academy of Sciences, v. 109, p. E1134–E1142, doi:10.1073/pnas.1116619109.

Davis, B.A.S., Brewer, S., Stevenson, A.C., and Guiot, J., 2003, The temperature of Europe during the Holocene reconstructed from pollen data: Quaternary Science Reviews, v. 22, p. 1701–1716, doi:10.1016/S0277-3791(03)00173-2.

Demény, A. et al., 2016, Recrystallization-induced oxygen isotope changes in inclusion-hosted water of speleothems – Paleoclimatological implications: Quaternary International, v. 415, p. 25–32, doi:10.1016/j.quaint.2015.11.137.

Demény, A., Rinyu, L., Kern, Z., Hatvani, I.G., Czuppon, G., Surányi, G., Leél-Őssy, S., Shen, C.-C., and Koltai, G., 2021, Paleotemperature reconstructions using speleothem fluid inclusion analyses from Hungary: Chemical Geology, v. 563, p. 120051, doi:10.1016/j.chemgeo.2020.120051.

Domínguez-Villar, D., Fairchild, I.J., Baker, A., Wang, X., Edwards, R.L., and Cheng, H., 2009, Oxygen isotope precipitation anomaly in the North Atlantic region during the 8.2 ka event: Geology, v. 37, p. 1095–1098, doi:10.1130/G30393A.1.

Domínguez-Villar, D., Wang, X., Krklec, K., Cheng, H., and Edwards, R.L., 2017, The control of the tropical North Atlantic on Holocene millennial climate oscillations: Geology, v. 45, p. 303–306, doi:10.1130/G38573.1.

Dublyansky, Y.V., and Spötl, C., 2009, Hydrogen and oxygen isotopes of water from inclusions in minerals: design of a new crushing system and on-line continuous-flow isotope ratio mass spectrometric analysis: Rapid Communications in Mass Spectrometry, v. 23, p. 2605–2613, doi:10.1002/rcm.4155.

Eynaud, F. et al., 2012, New constraints on European glacial freshwater releases to the North Atlantic Ocean: EUROPEAN GLACIAL FRESHWATER RELEASES: Geophysical Research Letters, v. 39, doi:10.1029/2012GL052100.

Fleitmann, D., Mudelsee, M., Burns, S.J., Bradley, R.S., Kramers, J., and Matter, A., 2008, Evidence for a widespread climatic anomaly at around 9.2 ka before present: CLIMATIC

ANOMALY AT AROUND 9.2 ka B.P.: Paleoceanography, v. 23, p. n/a-n/a, doi:10.1029/2007PA001519.

Fletcher, W.J. et al., 2010, Millennial-scale variability during the last glacial in vegetation records from Europe: Quaternary Science Reviews, v. 29, p. 2839–2864, doi:10.1016/j.quascirev.2009.11.015.

Fletcher, W.J., Debret, M., and Goñi, M.F.S., 2013, Mid-Holocene emergence of a low-frequency millennial oscillation in western Mediterranean climate: Implications for past dynamics of the North Atlantic atmospheric westerlies: The Holocene, v. 23, p. 153–166, doi:10.1177/0959683612460783.

García-Escárzaga, A. et al., 2022, Human forager response to abrupt climate change at 8.2 ka on the Atlantic coast of Europe: Scientific Reports, v. 12, p. 6481, doi:10.1038/s41598-022-10135-w.

García-Ruiz, J.M., Hughes, P.D., Palacios, D., and Andrés, N., 2023, The European glacial landscapes from the main deglaciation, *in* European Glacial Landscapes, Elsevier, p. 243–259, doi:10.1016/B978-0-323-91899-2.00032-2.

García-Ruiz, J.M., Palacios, D., Andrés, N., and López-Moreno, J.I., 2020, Neoglaciation in the Spanish Pyrenees: a multiproxy challenge: Mediterranean Geoscience Reviews, v. 2, p. 21–36, doi:10.1007/s42990-020-00022-9.

Genty, D., Blamart, D., Ghaleb, B., Plagnes, V., Causse, Ch., Bakalowicz, M., Zouari, K., Chkir, N., Hellstrom, J., and Wainer, K., 2006, Timing and dynamics of the last deglaciation from European and North African δ13C stalagmite profiles—comparison with Chinese and South Hemisphere stalagmites: Quaternary Science Reviews, v. 25, p. 2118–2142, doi:10.1016/j.quascirev.2006.01.030.

Giménez, R., Bartolomé, M., Gázquez, F., Iglesias, M., and Moreno, A., 2021, Underlying Climate Controls in Triple Oxygen (16 O, 17 O, 18 O) and Hydrogen (1 H, 2 H) Isotopes Composition of Rainfall (Central Pyrenees): Frontiers in Earth Science, v. 9, p. 633698, doi:10.3389/feart.2021.633698.

González-Sampériz, P. et al., 2017, Environmental and climate change in the southern Central Pyrenees since the Last Glacial Maximum: A view from the lake records: CATENA, v. 149, p. 668–688, doi:10.1016/j.catena.2016.07.041.

González-Sampériz, P., Valero-Garcés, B.L., Moreno, A., Jalut, G., García-Ruiz, J.M., Martí-Bono, C., Delgado-Huertas, A., Navas, A., Otto, T., and Dedoubat, J.J., 2006, Climate variability in the Spanish Pyrenees during the last 30,000 yr revealed by the El Portalet sequence: Quaternary Research, v. 66, p. 38–52, doi:10.1016/j.yqres.2006.02.004.

Heiri, O. et al., 2014a, Palaeoclimate records 60–8 ka in the Austrian and Swiss Alps and their forelands: Quaternary Science Reviews, v. 106, p. 186–205, doi:10.1016/j.quascirev.2014.05.021.

Heiri, O. et al., 2014b, Validation of climate model-inferred regional temperature change for late-glacial Europe: Nature Communications, v. 5, doi:10.1038/ncomms5914.

Honiat, C., Koltai, G., Dublyansky, Y., Edwards, R.L., Zhang, H., Cheng, H., and Spötl, C., 2023, A paleoprecipitation and paleotemperature reconstruction of the Last Interglacial in the southeastern Alps: Climate of the Past, v. 19, p. 1177–1199, doi:10.5194/cp-19-1177-2023.

Ilyashuk, E.A., Koinig, K.A., Heiri, O., Ilyashuk, B.P., and Psenner, R., 2011, Holocene temperature variations at a high-altitude site in the Eastern Alps: a chironomid record from Schwarzsee ob Sölden, Austria: Quaternary Science Reviews, v. 30, p. 176–191, doi:10.1016/j.quascirev.2010.10.008.

Iriarte-Chiapusso, M.J., 2016, Reviewing the Lateglacial-Holocene transition in NW Iberia: A palaeoecological approach based on the comparison between dissimilar regions: Quaternary International, p. 26.

Kilhavn, H., Couchoud, I., Drysdale, R.N., Rossi, C., Hellstrom, J., Arnaud, F., and Wong, H., 2022, The 8.2 ka event in northern Spain: timing, structure and climatic impact from a multi-proxy speleothem record: Climate of the Past, v. 18, p. 2321–2344, doi:10.5194/cp-18-2321-2022.

Kindler, P., Guillevic, M., Baumgartner, M., Schwander, J., Landais, A., and Leuenberger, M., 2014, Temperature reconstruction from 10 to 120 kyr b2k from the NGRIP ice core: Climate of the Past, v. 10, p. 887–902, doi:10.5194/cp-10-887-2014.

Kleiven, H. (Kikki) F., Kissel, C., Laj, C., Ninnemann, U.S., Richter, T.O., and Cortijo, E., 2008, Reduced North Atlantic Deep Water Coeval with the Glacial Lake Agassiz Freshwater Outburst: Science, v. 319, p. 60–64, doi:10.1126/science.1148924.

Lachniet, M.S., 2009, Climatic and environmental controls on speleothem oxygen-isotope values: Quaternary Science Reviews, v. 28, p. 412–432, doi:10.1016/j.quascirev.2008.10.021.

Landais, A., Capron, E., Masson-Delmotte, V., Toucanne, S., Rhodes, R., Popp, T., Vinther, B., Minster, B., and Prié, F., 2018, Ice core evidence for decoupling between midlatitude atmospheric water cycle and Greenland temperature during the last deglaciation: Climate of the Past, v. 14, p. 1405–1415, doi:10.5194/cp-14-1405-2018.

Larocque-Tobler, I., Heiri, O., and Wehrli, M., 2010, Late Glacial and Holocene temperature changes at Egelsee, Switzerland, reconstructed using subfossil chironomids: Journal of Paleolimnology, v. 43, p. 649–666, doi:10.1007/s10933-009-9358-z.

LeGrande, A.N., and Schmidt, G.A., 2008, Ensemble, water isotope-enabled, coupled general circulation modeling insights into the 8.2 ka event: ENSEMBLE, δ^{18}O GCM OF THE 8.2 KA EVENT: Paleoceanography, v. 23, p. n/a-n/a, doi:10.1029/2008PA001610.

Leunda, M. et al., 2019, Ice cave reveals environmental forcing of long-term Pyrenean tree line dynamics (B. Leys, Ed.): Journal of Ecology, v. 107, p. 814–828, doi:10.1111/1365-2745.13077.

Li, H., Spötl, C., and Cheng, H., 2020, A high-resolution speleothem proxy record of the Late Glacial in the European Alps: extending the NALPS19 record until the beginning of the Holocene: Journal of Quaternary Science, v. 36, p. 29–39, doi:10.1002/jqs.3255.

Lopez-Elorza, M., Muñoz-García, M.B., González-Acebrón, L., and Martín-Chivelet, J., 2021, Fluid-inclusion petrography in calcite stalagmites: Implications for entrapment processes: Journal of Sedimentary Research, v. 91, p. 1206–1226, doi:10.2110/jsr.2021.016.

Luetscher, M., Boch, R., Sodemann, H., Spötl, C., Cheng, H., Edwards, R.L., Frisia, S., Hof, F., and Müller, W., 2015, North Atlantic storm track changes during the Last Glacial Maximum recorded by Alpine speleothems: Nature Communications, v. 6, doi:10.1038/ncomms7344.

Marcott, S.A., Shakun, J.D., Clark, P.U., and Mix, A.C., 2013, A Reconstruction of Regional and Global Temperature for the Past 11,300 Years: Science, v. 339, p. 1198–1201, doi:10.1126/science.1228026.

Martrat, B., Jimenez-Amat, P., Zahn, R., and Grimalt, J.O., 2014, Similarities and dissimilarities between the last two deglaciations and interglaciations in the North Atlantic region: Quaternary Science Reviews, v. 99, p. 122–134, doi:10.1016/j.quascirev.2014.06.016.

Masson-Delmotte, V., Jouzel, J., Landais, A., Stievenard, M., Johnsen, S.J., White, J.W.C., Werner, M., Sveinbjornsdottir, A., and Fuhrer, K., 2005, GRIP Deuterium Excess Reveals Rapid and Orbital-Scale Changes in Greenland Moisture Origin: Science, v. 309, p. 118–121, doi:10.1126/science.1108575.

Matero, I.S.O., Gregoire, L.J., Ivanovic, R.F., Tindall, J.C., and Haywood, A.M., 2017, The 8.2 ka cooling event caused by Laurentide ice saddle collapse: Earth and Planetary Science Letters, v. 473, p. 205–214, doi:10.1016/j.epsl.2017.06.011.

McDermott, F., 2004, Palaeo-climate reconstruction from stable isotope variations in speleothems: a review: Quaternary Science Reviews, v. 23, p. 901–918, doi:10.1016/j.quascirev.2003.06.021.

Mesa-Fernández, J.M., Jiménez-Moreno, G., Rodrigo-Gámiz, M., García-Alix, A., Jiménez-Espejo, F.J., Martínez-Ruiz, F., Anderson, R.S., Camuera, J., and Ramos-Román, M.J., 2018, Vegetation and geochemical responses to Holocene rapid climate change in the Sierra Nevada (southeastern Iberia): the Laguna Hondera record: Climate of the Past, v. 14, p. 1687–1706, doi:10.5194/cp-14-1687-2018.

Millet, L., Rius, D., Galop, D., Heiri, O., and Brooks, S.J., 2012, Chironomid-based reconstruction of Lateglacial summer temperatures from the Ech palaeolake record (French western Pyrenees): Palaeogeography, Palaeoclimatology, Palaeoecology, v. 315–316, p. 86–99, doi:10.1016/j.palaeo.2011.11.014.

Morellón, M., Aranbarri, J., Moreno, A., González-Sampériz, P., and Valero-Garcés, B.L., 2018, Early Holocene humidity patterns in the Iberian Peninsula reconstructed from lake, pollen and speleothem records: Quaternary Science Reviews, v. 181, p. 1–18, doi:10.1016/j.quascirev.2017.11.016.

Moreno, A. et al., 2014, A compilation of Western European terrestrial records 60–8 ka BP: towards an understanding of latitudinal climatic gradients: Quaternary Science Reviews, v. 106, p. 167–185, doi:10.1016/j.quascirev.2014.06.030.

Moreno, A. et al., 2021, Measurement report: Spatial variability of northern Iberian rainfall stable isotope values – investigating atmospheric controls on daily and monthly timescales: Atmospheric Chemistry and Physics, v. 21, p. 10159–10177, doi:10.5194/acp-21-10159-2021.

Moreno, A., Pérez-Mejías, C., Bartolomé, M., Sancho, C., Cacho, I., Stoll, H., Delgado-Huertas, A., Hellstrom, J., Edwards, R.L., and Cheng, H., 2017, New speleothem data from Molinos and Ejulve caves reveal Holocene hydrological variability in northeast Iberia: Quaternary Research, v. 88, p. 223–233, doi:10.1017/qua.2017.39.

Morrill, C., Anderson, D.M., Bauer, B.A., Buckner, R., Gille, E.P., Gross, W.S., Hartman, M., and Shah, A., 2013, Proxy benchmarks for intercomparison of 8.2 ka simulations: Climate of the Past, v. 9, p. 423–432, doi:10.5194/cp-9-423-2013.

Muñoz Sobrino, C., Heiri, O., Hazekamp, M., van der Velden, D., Kirilova, E.P., García-Moreiras, I., and Lotter, A.F., 2013, New data on the Lateglacial period of SW Europe: a high resolution multiproxy record from Laguna de la Roya (NW Iberia): Quaternary Science Reviews, v. 80, p. 58–77, doi:10.1016/j.quascirev.2013.08.016.

Nebout, N.C., Peyron, O., Dormoy, I., Desprat, S., Beaudouin, C., Kotthoff, U., and Marret, F., 2009, Rapid climatic variability in the west Mediterranean during the last 25 000 years from high resolution pollen data: Clim. Past, p. 19.

Pérez-Mejías, C., Moreno, A., Bernal-Wormull, J., Cacho, I., Osácar, M.C., Edwards, R.L., and Cheng, H., 2021, Oldest Dryas hydroclimate reorganization in the eastern Iberian Peninsula after the iceberg discharges of Heinrich Event 1: Quaternary Research, v. 101, p. 67–83, doi:10.1017/qua.2020.112.

Poage, M.A., 2001, Empirical relationships between elevation and the stable isotope composition of precipitation and surface waters: considerations for studies of paleoelevation change: American Journal of Science, v. 301, p. 1–15, doi:10.2475/ajs.301.1.1.

Rasmussen, S.O. et al., 2014, A stratigraphic framework for abrupt climatic changes during the Last Glacial period based on three synchronized Greenland ice-core records: refining and extending the INTIMATE event stratigraphy: Quaternary Science Reviews, v. 106, p. 14–28, doi:10.1016/j.quascirev.2014.09.007.

Rasmussen, S.O., Vinther, B.M., Clausen, H.B., and Andersen, K.K., 2007, Early Holocene climate oscillations recorded in three Greenland ice cores: Quaternary Science Reviews, v. 26, p. 1907–1914, doi:10.1016/j.quascirev.2007.06.015.

Renssen, H., and Isarin, R.F.B., 2001, The two major warming phases of the last deglaciation at ~14.7 and ~11.5 ka cal BP in Europe: climate reconstructions and AGCM experiments: Global and Planetary Change, v. 30, p. 117–153, doi:10.1016/S0921-8181(01)00082-0.

Rodrigo-Gámiz, M., García-Alix, A., Jiménez-Moreno, G., Ramos-Román, M.J., Camuera, J., Toney, J.L., Sachse, D., Anderson, R.S., and Sinninghe Damsté, J.S., 2022, Paleoclimate reconstruction of the last 36 kyr based on branched glycerol dialkyl glycerol tetraethers in the Padul palaeolake record (Sierra Nevada, southern Iberian Peninsula): Quaternary Science Reviews, v. 281, p. 107434, doi:10.1016/j.quascirev.2022.107434.

https://doi.org/10.5194/egusphere-2024-3612
Preprint. Discussion started: 26 November 2024

Rodrigues, T., Grimalt, J.O., Abrantes, F., Naughton, F., and Flores, J.-A., 2010, The last glacial–interglacial transition (LGIT) in the western mid-latitudes of the North Atlantic: Abrupt sea surface temperature change and sea level implications: Quaternary Science Reviews, v. 29, p. 1853–1862, doi:10.1016/j.quascirev.2010.04.004.

Rossi, C., Bajo, P., Lozano, R.P., and Hellstrom, J., 2018, Younger Dryas to Early Holocene paleoclimate in Cantabria (N Spain): Constraints from speleothem Mg, annual fluorescence banding and stable isotope records: Quaternary Science Reviews, v. 192, p. 71–85, doi:10.1016/j.quascirev.2018.05.025.

Rozanski, K., Araguás-Araguás, L., and Gonfiantini, R., 1993, Isotopic Patterns in Modern Global Precipitation, *in* Swart, P.K., Lohmann, K.C., Mckenzie, J., and Savin, S. eds., Geophysical Monograph Series, Washington, D. C., American Geophysical Union, p. 1–36, doi:10.1029/GM078p0001.

Rozanski, K., Araguás-Araguás, L., and Gonfiantini, R., 1992, Relation Between Long-Term Trends of Oxygen-18 Isotope Composition of Precipitation and Climate: Science, v. 258, p. 981–985, doi:10.1126/science.258.5084.981.

Sancho, C., Belmonte, Á., Bartolomé, M., Moreno, A., Leunda, M., and López-Martínez, J., 2018, Middle-to-late Holocene palaeoenvironmental reconstruction from the A294 ice-cave record (Central Pyrenees, northern Spain): Earth and Planetary Science Letters, v. 484, p. 135–144, doi:10.1016/j.epsl.2017.12.027.

Seierstad, I.K. et al., 2014, Consistently dated records from the Greenland GRIP, GISP2 and NGRIP ice cores for the past 104 ka reveal regional millennial-scale δ18O gradients with possible Heinrich event imprint: Quaternary Science Reviews, v. 106, p. 29–46, doi:10.1016/j.quascirev.2014.10.032.

Shakun, J.D., 2018, Pollen weighs in on a climate conundrum: Nature, v. 554, p. 39–40, doi:10.1038/d41586-018-00943-4.

Skinner, L.C., and Shackleton, N.J., 2006, Deconstructing Terminations I and II: revisiting the glacioeustatic paradigm based on deep-water temperature estimates: Quaternary Science Reviews, v. 25, p. 3312–3321, doi:10.1016/j.quascirev.2006.07.005.

Tarrats, P., Heiri, O., Valero-Garcés, B., Cañedo-Argüelles, M., Prat, N., Rieradevall, M., and González-Sampériz, P., 2018, Chironomid-inferred Holocene temperature reconstruction in Basa de la Mora Lake (Central Pyrenees): The Holocene, v. 28, p. 1685–1696, doi:10.1177/0959683618788662.

Uemura, R., Kina, Y., Shen, C.-C., and Omine, K., 2020, Experimental evaluation of oxygen isotopic exchange between inclusion water and host calcite in speleothems: Climate of the Past, v. 16, p. 17–27, doi:10.5194/cp-16-17-2020.

Van Raden, U.J., Colombaroli, D., Gilli, A., Schwander, J., Bernasconi, S.M., Van Leeuwen, J., Leuenberger, M., and Eicher, U., 2013, High-resolution late-glacial chronology for the Gerzensee lake record (Switzerland): δ18O correlation between a Gerzensee-stack and NGRIP: Palaeogeography, Palaeoclimatology, Palaeoecology, v. 391, p. 13–24, doi:10.1016/j.palaeo.2012.05.017.

Vegas, J., Ruiz-Zapata, B., Ortiz, J.E., Galán, L., Torres, T., García-Cortés, Á., Gil-García, M.J., Pérez-González, A., and Gallardo-Millán, J.L., 2010, Identification of arid phases during the last 50 cal. ka BP from the Fuentillejo maar-lacustrine record (Campo de Calatrava Volcanic Field, Spain): ARID PHASES DURING THE LAST 50 KA FROM THE FUENTILLEJO MAAR-LAKE RECORD, SPAIN: Journal of Quaternary Science, v. 25, p. 1051–1062, doi:10.1002/jqs.1262.

Vegas-Vilarrúbia, T., González-Sampériz, P., Morellón, M., Gil-Romera, G., Pérez-Sanz, A., and Valero-Garcés, B., 2013, Diatom and vegetation responses to Late Glacial and Early Holocene climate changes at Lake Estanya (Southern Pyrenees, NE Spain): Palaeogeography, Palaeoclimatology, Palaeoecology, v. 392, p. 335–349, doi:10.1016/j.palaeo.2013.09.011.

Von Grafenstein, U., Belmecheri, S., Eicher, U., Van Raden, U.J., Erlenkeuser, H., Andersen, N., and Ammann, B., 2013, The oxygen and carbon isotopic signatures of biogenic carbonates in Gerzensee, Switzerland, during the rapid warming around 14,685years BP and the following interstadial: Palaeogeography, Palaeoclimatology, Palaeoecology, v. 391, p. 25–32, doi:10.1016/j.palaeo.2013.08.018.

Von Grafenstein, U., Erlenkeuser, H., Brauer, A., Jouzel, J., and Johnsen, S., 1999, A mid-European decadal isotope-climate record from 15,500 to 5000 years B.P.: Science, v. 284, p. 1654–1657, doi:10.1126/science.284.5420.1654.

Vonhof, H.B., van Breukelen, M.R., Postma, O., Rowe, P.J., Atkinson, T.C., and Kroon, D., 2006, A continuous-flow crushing device for on-line$\delta 2H$ analysis of fluid inclusion water in speleothems: Rapid Communications in Mass Spectrometry, v. 20, p. 2553–2558, doi:10.1002/rcm.2618.

Wanner, H. et al., 2008, Mid- to Late Holocene climate change: an overview: Quaternary Science Reviews, v. 27, p. 1791–1828, doi:10.1016/j.quascirev.2008.06.013.

Wanner, H., Solomina, O., Grosjean, M., Ritz, S.P., and Jetel, M., 2011, Structure and origin of Holocene cold events: Quaternary Science Reviews, v. 30, p. 3109–3123, doi:10.1016/j.quascirev.2011.07.010.

Wilcox, P.S., Honiat, C., Trüssel, M., Edwards, R.L., and Spötl, C., 2020, Exceptional warmth and climate instability occurred in the European Alps during the Last Interglacial period: Communications Earth & Environment, v. 1, p. 57, doi:10.1038/s43247-020-00063-w.

Zielhofer, C., Köhler, A., Mischke, S., Benkaddour, A., Mikdad, A., and Fletcher, W.J., 2019, Western Mediterranean hydro-climatic consequences of Holocene ice-rafted debris (Bond) events: Climate of the Past, v. 15, p. 463–475, doi:10.5194/cp-15-463-2019.

https://doi.org/10.5194/egusphere-2024-3612
Preprint. Discussion started: 26 November 2024

FIGURE CAPTIONS

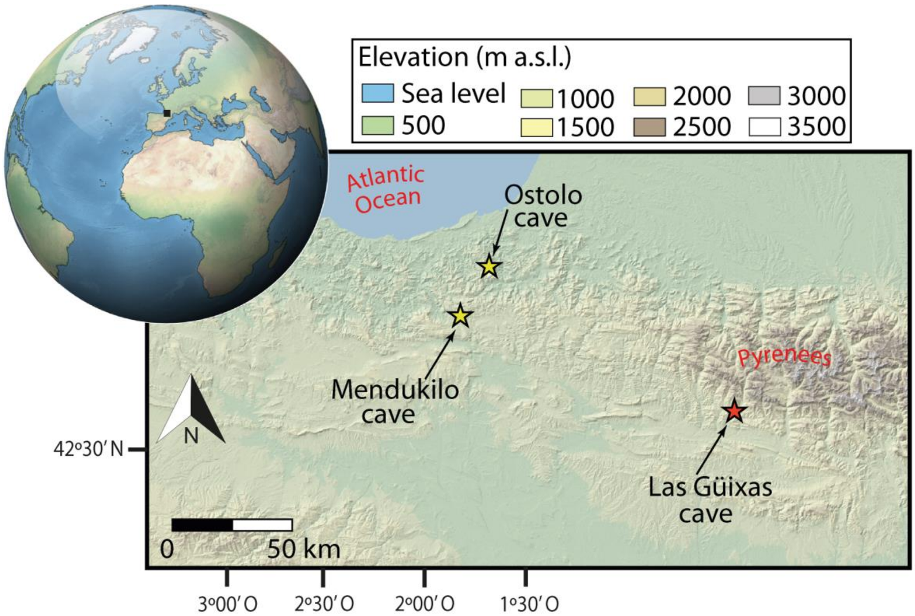

Figure 1. Location of the study area in Northern Spain. Yellow stars indicate the locations of the two studied caves, while the red star marks the site where the isotopic composition of rainfall was monitored (Las Güixas tourist cave in Villanúa).

https://doi.org/10.5194/egusphere-2024-3612
Preprint. Discussion started: 26 November 2024

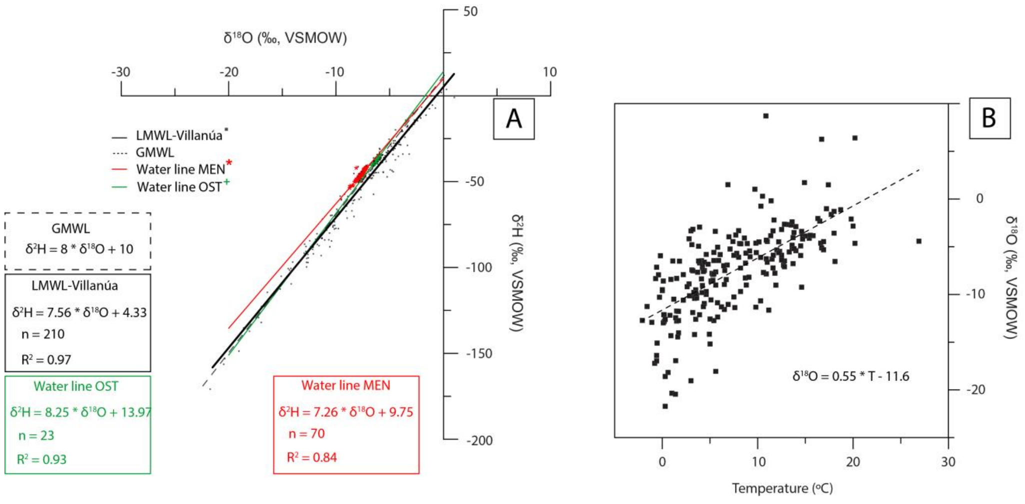

Figure 2. A) δ^2H and δ^{18}O values of precipitation events at Villanúa (black dots) along with the Local Meteoric Water Line (LMWL; black line). Samples that experienced evaporation prior to sampling and outliers were excluded (Giménez et al., 2021). The Global Meteoric Water Line (GMWL; dashed line; Rozanski et al., 1993) and the drip water lines of Mendukilo (MEN; red line) and Ostolo (OST; green line) are also represented. B) δ^{18}O values of precipitation events and their respective temperature at Villanúa (Giménez et al., 2021). The dashed line represents the linear regression of precipitation isotope and temperature data.

https://doi.org/10.5194/egusphere-2024-3612
Preprint. Discussion started: 26 November 2024

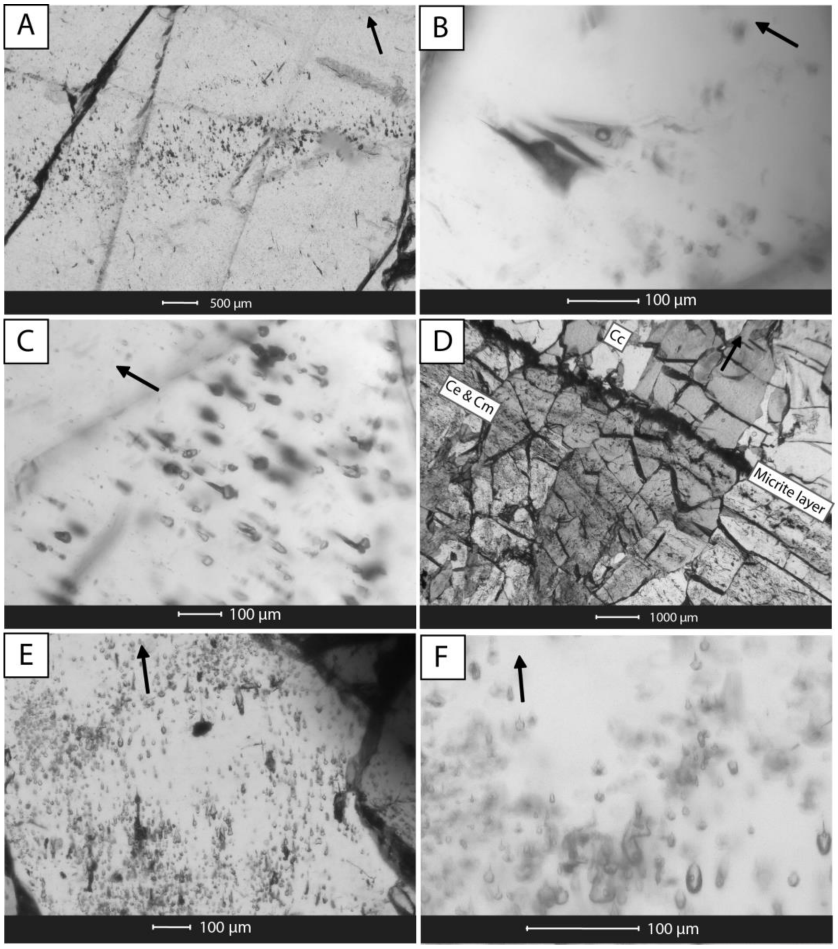

Figure 3. FI assemblages in the studied stalagmites. A) Primary FI throughout the growth layers in stalagmite MEN-5. B) Inter-crystalline FI in stalagmite MEN-2. C) Intra-crystalline FI in stalagmite MEN-5. D) Primary intra and inter-crystalline FI in stalagmite OST2, more frequently found in porous areas or associated with elongated (Ce) and/or microcrystalline (Cm) fabrics than with a tightly packed columnar fabric (Cc). E) FI in stalagmite OST2 are mostly intra-crystalline and does not necessarily align with the growth layers. F) Pyriform and rounded intra-crystalline small FI in stalagmite OST2. Black arrows indicate the speleothem growth direction.

https://doi.org/10.5194/egusphere-2024-3612
Preprint. Discussion started: 26 November 2024

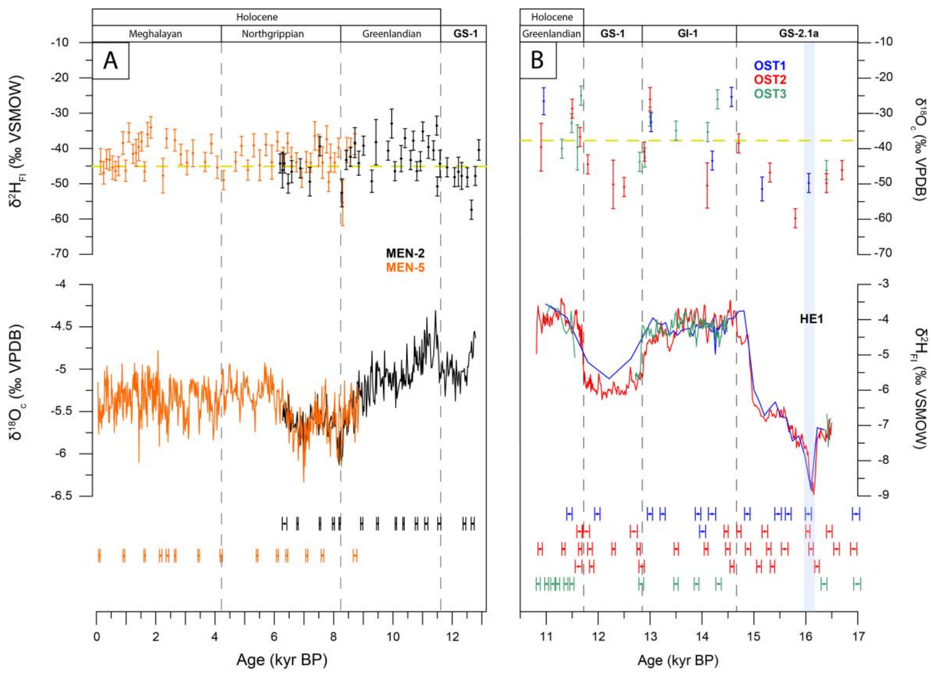

Figure 4. A) δ^2H of FI water (δ^2H_{FI}) and δ^{18}O of calcite ($\delta^{18}O_c$) of Mendukilo (MEN-5 in orange and MEN-2 in black) and B) Ostolo stalagmites (OST1 in blue, OST2 in red, and OST3 in green). δ^2H_{FI} values are corrected for the ice-volume effect (Bintanja et al., 2005) with vertical error bars representing isotope measurements errors and 1σ from repeated measurements. The yellow dashed line in the upper graphs of each panel indicates the annual mean δ^2H value in drip water for each cave. Modeled U/Th ages with 2σ error bars for stalagmites from each cave are shown at the bottom. Heinrich event 1 (HE1) recorded in the Ostolo isotope record (Bernal-Wormull et al., 2021) is highlighted by a light blue bar.

https://doi.org/10.5194/egusphere-2024-3612
Preprint. Discussion started: 26 November 2024

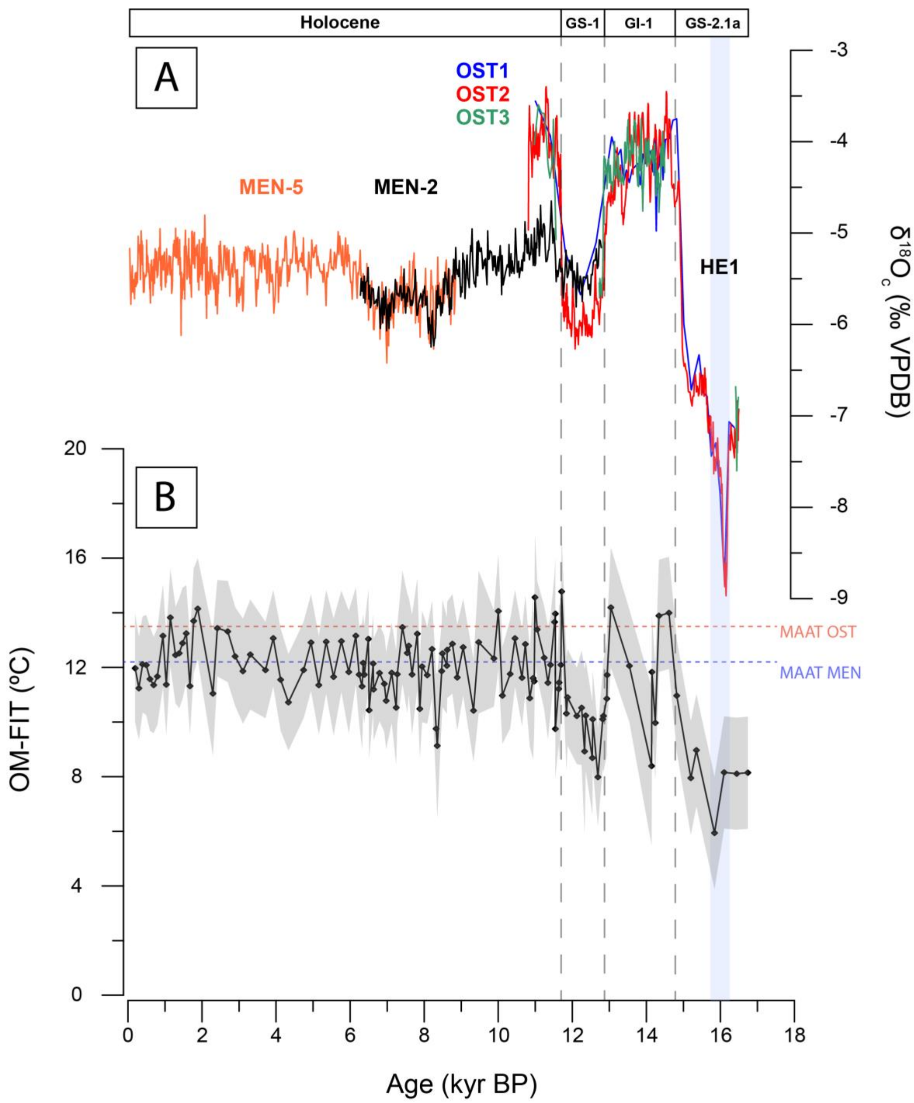

Figure 5. A) $\delta^{18}O_c$ records from Mendukilo and Ostolo stalagmites, compared to B) the OM-FIT paleotemperature reconstruction (bottom). Heinrich event 1 (HE1) is highlighted by a light blue bar. The MAAT outside the two caves is shown by dashed horizontal lines.

https://doi.org/10.5194/egusphere-2024-3612
Preprint. Discussion started: 26 November 2024

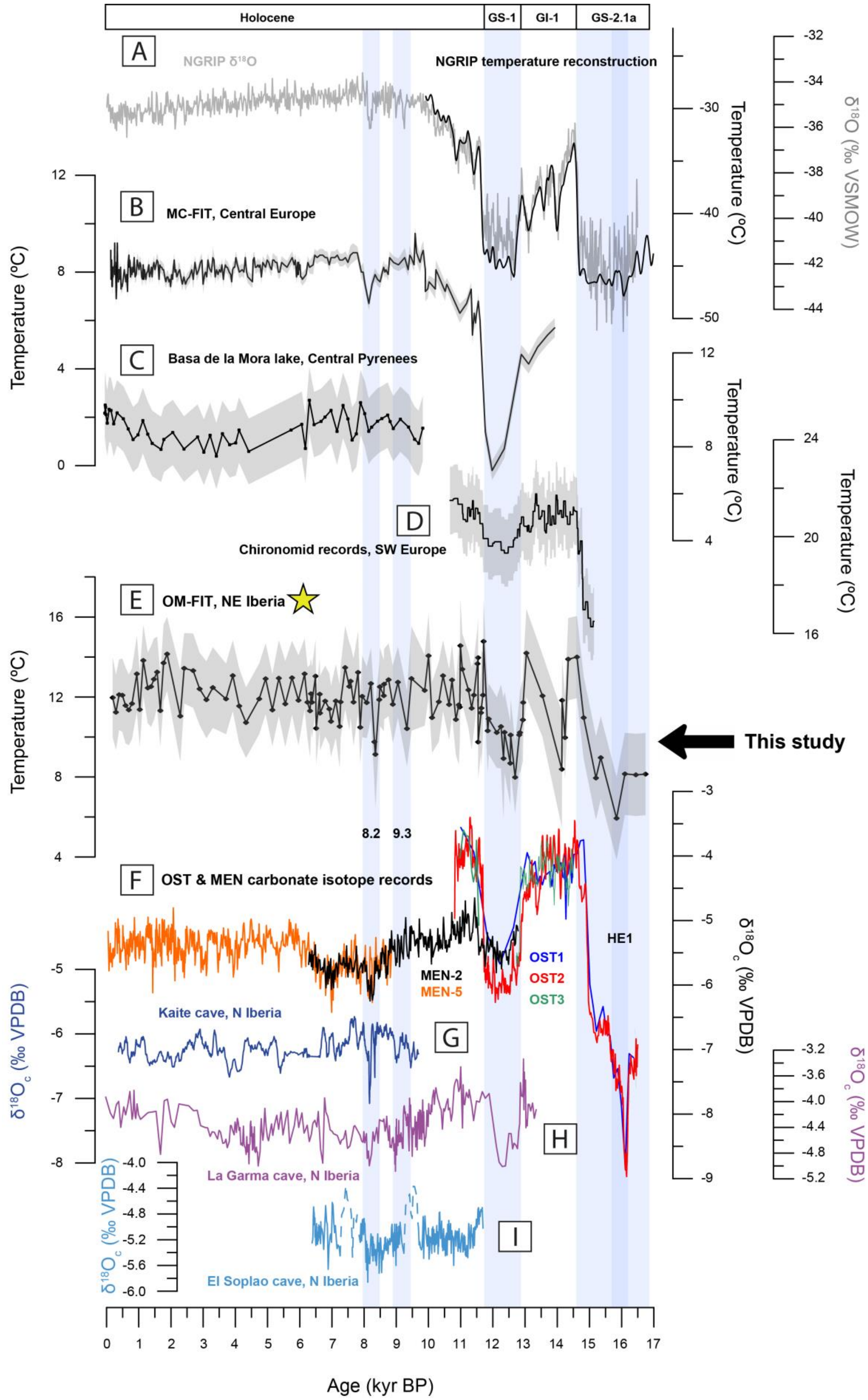

https://doi.org/10.5194/egusphere-2024-3612
Preprint. Discussion started: 26 November 2024

Figure 6. Paleotemperature reconstructions over the last 16.5 kyr BP, spanning from Greenland to SW Europe, along with speleothem $\delta^{18}O$ records from the Iberian Peninsula. A) NGRIP $\delta^{18}O$ (gray solid line; Rasmussen et al., 2014) and Greenland temperature reconstruction (black solid line; Kindler et al., 2014). B) Milandre cave FI temperature record (MC-FIT) from NW Switzerland (Affolter et al., 2019). C) July temperature inferred from chironomids at Basa de la Mora Lake (Tarrats et al., 2018). D) Stacked and spliced chironomid-inferred July temperature record from SW Europe (Heiri et al., 2014b). E) Ostolo and Mendukilo FI temperature record (OM-FIT; yellow star; this study). F) $\delta^{18}O_c$ records from Mendukilo and Ostolo (Bernal-Wormull et al., 2021, 2023). G) LV5 $\delta^{18}O$ record from Kaite Cave (northern Iberia; Domínguez-Villar et al., 2017). H) GAR-01 $\delta^{18}O$ record from La Garma Cave (northern Iberia; Baldini et al., 2019). I) SIR-14 $\delta^{18}O$ record from El Soplao Cave (northern Iberia; Kilhavn et al., 2022). Key abrupt climate events (Heinrich 1 [HE1], 9.3 kyr and the 8.2 kyr events) and Greenland stadials (GS-1 and GS-2.1a) are highlighted by a light blue bar. The gray envelope around the solid lines in B), C), D) and E) show the uncertainties.